Decreased cortical bone mass and diminished bone rigidity in the tibia of Glp-1r $^{-/-}$ mice

To evaluate the impact of the lack of GLP-1 receptor signaling on bone mass, we performed CT-based bone densitometry in bones of differing cortical/cancellous bone ratio. Tibia and lumber spine were used because the former has a higher cortical/cancellous bone ratio, whereas the latter has a lower cortical/cancellous bone ratio. The results are shown as total, cortical, cancellous, and trabecular bone mass in Fig. 1. There was no significant difference between WT and Glp-1r $^{-/-}$ mice in BMC (milligrams) (Fig. 1, A–D) and bone volume (cubic centimeters) (Fig. 1, E–H). Total BMD of tibia was significantly lower in Glp-1r$^{-/-}$ mice than in WT mice (WT mice, 612.97 ± 4.03 mg/cm^3; Glp-1r$^{-/-}$ mice, 570.07 ± 4.22 mg/cm^3; P = 0.0000036), but no significant difference was observed in total BMD of spine (Fig. 2I). Cortical BMD also was significantly decreased in Glp-1r $^{-/-}$ mice compared with WT mice in both tibia and spine (tibia: WT mice, 687.34 ± 3.57 mg/cm^3; Glp-1r $^{-/-}$ mice, 650.06 ± 10.59 mg/cm^3; P = 0.0093; spine: WT mice, 411.31 ± 8.77 mg/cm^3; Glp-1r $^{-/-}$ mice, 380.45 ± 6.67 mg/cm^3; P = 0.018) (Fig. 1J). However, cancellous and trabecular BMD were not significantly different in WT and Glp-1r $^{-/-}$ mice in both tibia and spine (Fig. 1, K and L). Reflecting the loss of cortical bone, Glp-1r$^{-/-}$ mice showed skeletal fragility by diminished bone rigidity indexes. The minimum moment of inertia of cross-sectional areas, which represents flexural rigidity, was significantly reduced in Glp-1r$^{-/-}$ mice (WT mice, 0.014 ± 0.002 mg·cm; Glp-1r$^{-/-}$ mice, 0.008 ± 0.001 mg·cm; P = 0.022) (Fig. 1M). Moreover, torsional rigidity as indicated by the polar moment of inertia of cross-sectional areas also was significantly diminished in Glp-1r$^{-/-}$ mice (WT mice, 0.064 ± 0.006 mg·cm; Glp-1r$^{-/-}$ mice, 0.040 ± 0.006 mg·cm; P = 0.020) (Fig. 1N). These results indicate that Glp-1r $^{-/-}$ mice have cortical osteopenia and bone fragility.

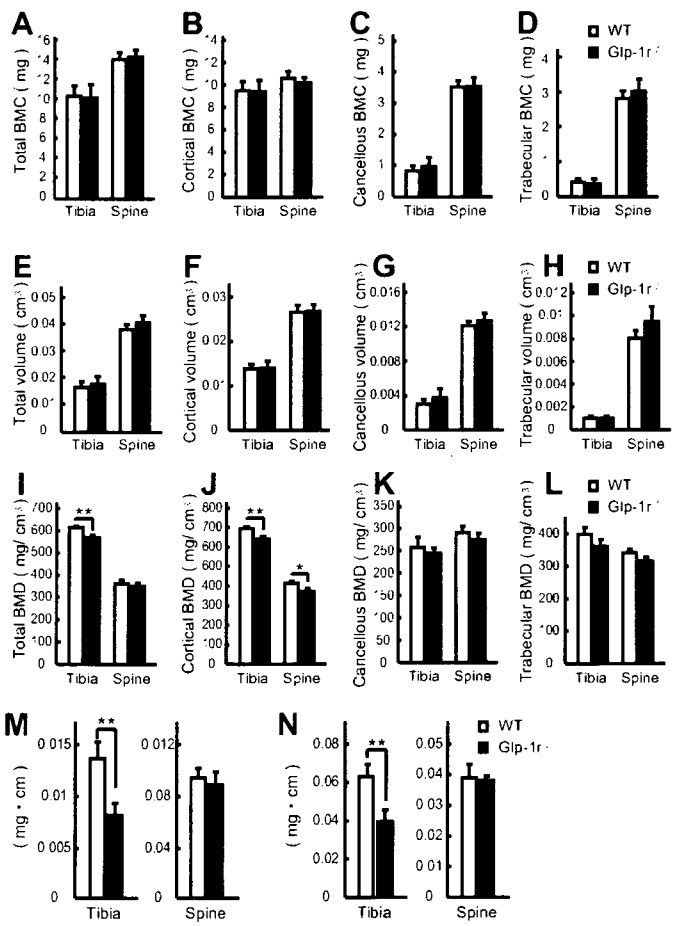

FIG. 1. CT-based bone densitometry of tibia and lumbar spine in 10-wk-old male WT (*white bars*) and Glp-1r$^{-/-}$ (*black bars*) mice. A–D, Total (A), cortical (B), cancellous (C), and trabecular (D) BMC; E–H, total (E), cortical (F), cancellous (G), and trabecular (H) BV; I–L, total (I), cortical (J), cancellous (K), and trabecular (L) BMD; M, minimum moment of inertia of cross-sectional areas, representing the flexural rigidity; N, the polar moment of inertia of cross-sectional areas, representing the torsional rigidity, calculated by LaTheta software. Values are expressed as means ± SE; n = 6 mice per group. *, $P < 0.05$; **, $P < 0.01$, WT *vs.* Glp-1r$^{-/-}$ mice.

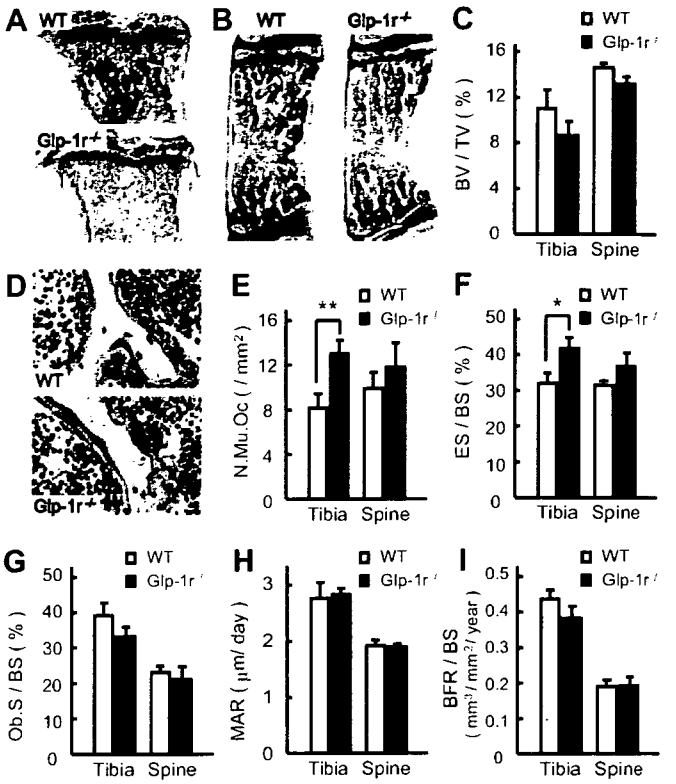

FIG. 2. Bone histomorphometry of tibia and lumbar spine in 6-wk-old male WT (*white bars*) and Glp-1r$^{-/-}$ (*black bars*) mice. A, Representative pictures of proximal tibia. Original magnification, ×20. B, Representative pictures of lumbar spine. Original magnification, ×40. C, BV/TV of tibia and lumbar spine in WT and Glp-1r $^{-/-}$ mice. D, Multinuclear osteoclasts in WT and Glp-1r$^{-/-}$ mice. Original magnification, ×400. E and F, N.Mu.Oc (E) and ES/BS (F) as cellular activity parameters regarding bone resorption. G–I, Osteoblast surface (Ob.S)/BS (G), mineral apposition rate (MAR) (H), and bone formation rate (BFR)/BS (I) as bone formation parameters. Values are expressed as means ± SE; n = 5–7 mice per group. *, $P < 0.05$; **, $P < 0.01$, WT *vs.* Glp-1r$^{-/-}$ mice.

Glp-1r$^{-/-}$ mice exhibit increased numbers of osteoclasts and bone resorption activity in the tibiae

We next performed histomorphometrical analyses of proximal tibiae (Fig. 2A) and lumbar spines (Fig. 2B) of 6-wk-old

male WT and Glp-1r$^{-/-}$ mice. Although the bone volume (BV)/tissue volume (TV) ratio (Fig. 2C) was somewhat lower in Glp-1r$^{-/-}$ mice in both tibia and spine, the difference was not statistically significant. The number of osteoclasts (N.Oc), especially multinuclear osteoclasts (N.Mu.Oc), the fully differentiated cells responsible for active bone resorption, was significantly increased in tibia of Glp-1r$^{-/-}$ mice (Fig. 2, D and E), and all of the following parameters indicating osteoclastic number were also significantly higher in the tibia of Glp-1r$^{-/-}$ mice: N.Mu.Oc per bone surface (BS) (2.06/mm^2 *vs.* 3.90/mm^2, $P = 0.022$), N.Mu.Oc per eroded surface (ES) (6.18/mm^2 *vs.* 9.32/mm^2, $P = 0.040$), N.Mu.Oc/TV (12.22/mm^2 *vs.* 20.26/mm^2, $P = 0.012$), N.Oc/BS (3.21/mm^2 *vs.* 5.98/mm^2, $P = 0.002$), and N.Oc/TV (19.28/mm^2 *vs.* 31.59/mm^2, $P = 0.009$), for WT *vs.* Glp-1r$^{-/-}$ mice, respectively. Furthermore, eroded surface (ES/BS) was significantly increased in the tibiae of Glp-1r$^{-/-}$ mice compared with WT mice (Fig. 2F). However, osteoclastic bone resorption activity was less apparent in spine of Glp-1r$^{-/-}$ mice (Fig. 2, E and F). On the other hand, no significant difference was observed in bone formation parameters, including osteoblast surface per BS (Fig. 2G), mineral apposition rate (Fig. 2H), and bone formation rate (Fig. 2I) between WT and Glp-1r$^{-/-}$ mice.

GLP-1 has no direct effect on osteoclasts and osteoblasts

Because osteoclastic number and bone resorptive activity were increased in Glp-1r$^{-/-}$ mice, we investigated whether GLP-1 has a direct effect on osteoclasts and/or osteoblasts using cell culture models. We first evaluated the effect of GLP-1 on osteoclastic differentiation by culturing bone marrow cells together with osteoblasts, because osteoclasts are formed from the precursor cells in bone marrow by stimulation from osteoblasts. As a result, GLP-1 had no inhibitory effect on 1α,25-dihydroxyvitamin D_3-induced osteoclastic generation (Fig. 3A). Pit-forming assays showed that GLP-1 had no direct effect on pit-forming activity of mature osteoclasts placed on dentine slices, whereas calcitonin completely inhibited pit formation (Fig. 3B). Unlike the GIP receptor, the GLP-1 receptor was absent in osteoblasts, and GLP-1failed to increase intracellular cAMP levels in Saos-2 cells (data not shown). Furthermore, GLP-1 had no protective effect on etoposide-induced osteoblastic apoptosis (Fig. 3C). These *in vitro* experiments demonstrate that GLP-1 has no direct effect on either osteoclasts or osteoblasts.

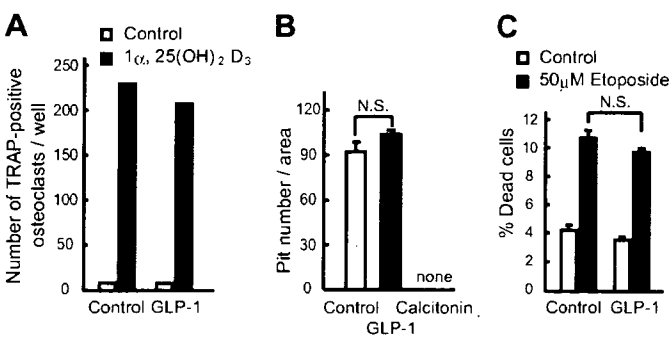

FIG. 3. Effects of GLP-1 on osteoclasts and osteoblasts *in vitro*. A, Effect of GLP-1 on osteoclastic differentiation. The numbers of tartrate-resistant acid phosphatase (TRAP)-positive osteoclasts formed from coculture of osteoblasts and bone marrow cells in the presence or absence of 10^{-8} M 1α,25-dihydroxyvitamin D_3 [1α, 25(OH)$_2$ D_3] (*white bars*)and/or 10^{-5} M GLP-1 (*black bars*) are shown. B, Effect of GLP-1 on the pit-forming activity of mature osteoclasts, using 10^{-10} M calcitonin as a positive control. C, Effect of GLP-1 on osteoblastic apoptosis. Saos-2 cells were pretreated with 10^{-4} M GLP-1 for 1 h and then incubated for an additional 6 h in the absence (*white bars*) or presence of 50 μM etoposide (*black bars*). Values are expressed as means ± SE.

GLP-1 receptor signaling modulates calcitonin expression in mice

Because GLP-1 has no direct effect on bone cells, we investigated indirect pathways of GLP-1-mediated bone metabolism. Plasma levels of total calcium (data not shown) and ionized calcium (Fig. 4A) were unchanged in both fasting and fed conditions. Because hyperparathyroidism is a cause of cortical bone loss, plasma intact PTH levels were measured, but there was no difference in PTH levels between WT and Glp-1r$^{-/-}$ mice (Fig. 4B). Because the GLP-1 receptor is expressed in thyroid C cells and GLP-1 stimulates calcitonin secretion *in vitro* via a cAMP-mediated mechanism (10, 11), calcitonin could be involved in the alteration of bone metabolism observed in Glp-1r$^{-/-}$ mice. Quantitative real-time PCR analysis revealed that administration of the GLP-1 receptor agonist exendin-4 significantly increased thyroid calcitonin mRNA levels in WT mice (Fig. 4C). Conversely, the loss of GLP-1 receptor signaling in Glp-1r$^{-/-}$ mice was as-

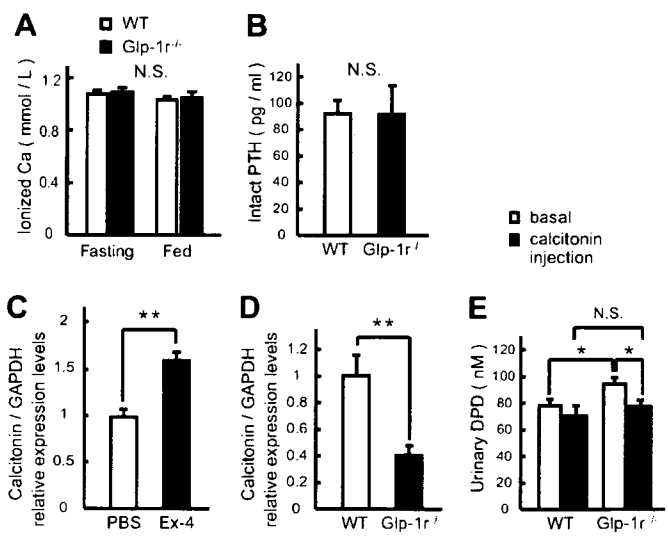

FIG. 4. Calcitonin deficiency resulted in increased bone resorption in Glp-1r$^{-/-}$ mice. A and B, Plasma levels of ionized calcium (A) and intact PTH (B) in WT and Glp-1r$^{-/-}$ mice. Values are expressed as means ± SE; n = 6–8 mice per group. C, Relative expression levels of calcitonin mRNA in thyroid from WT mice injected ip with PBS or 24 nmol/kg exendin-4 (Ex-4) 6 h before RNA isolation. Values are expressed as means ± SE; n = 5 mice per group. *, $P < 0.01$, PBS *vs.* exendin-4 treatment. D, Relative expression levels of calcitonin mRNA in thyroid from WT and Glp-1r$^{-/-}$ mice determined by quantitative real-time PCR. Values are expressed as means ± SE; n = 4 mice per group. *, $P < 0.05$; **, $P < 0.01$, WT *vs.* Glp-1r$^{-/-}$ mice. E, Urinary elimination of DPD from WT and Glp-1r$^{-/-}$ mice before and at 4 h after single administration of 10 IU/kg calcitonin. Values are expressed as means ± SE; n = 6 mice per group. *, $P < 0.05$, WT *vs.* Glp-1r$^{-/-}$ mice.

sociated with a significant reduction in levels of calcitonin mRNA transcripts, 41% of levels in control WT thyroid glands (Fig. 4D). Consistent with results of bone histomorphometry showing increased osteoclastic bone resorption, Glp-1r$^{-/-}$ mice showed significantly higher urinary DPD concentration (Fig. 4E). However, calcitonin treatment effectively decreased the urinary DPD concentration in Glp-1r$^{-/-}$ mice (Fig. 4E), demonstrating that increased bone resorption in Glp-1r$^{-/-}$ mice remains sensitive to the antiresorptive actions of calcitonin.

Discussion

Decreased BMD is a major determinant of fracture, but fracture risk in diabetic patients is often increased (17–19) and is not necessarily associated with decreased BMD. BMD in type 2 diabetes has been reported to be decreased, normal, or increased depending on various factors such as body weight or the site where BMD is measured. Body weight is one of the main determinants of BMD in both diabetic and nondiabetic subjects, suggesting that the increased BMD could be explained by the higher body weight. In the present study, there was no difference in several metabolic factors that often indirectly modulate BMD, including body weight, fat mass, or plasma levels of leptin, between WT and Glp-1r$^{-/-}$ mice.

Quantitative CT was used in the present study for the measurement of BMD because of the merits of the method with regard to distinct assessment of cortical, cancellous, and trabecular bones and to providing indexes of bone strength in live animals (13, 20). We found that total BMD of tibia, which has a higher cortical/cancellous bone ratio, was significantly lower in Glp-1r$^{-/-}$ mice and that cortical BMD at both tibia and lumbar spine was selectively reduced in Glp-1r$^{-/-}$ mice compared with WT mice. Reflecting the cortical bone loss, Glp-1r$^{-/-}$ mice showed skeletal fragility. In diabetic patients, BMD measured at sites with high cortical/cancellous bone ratio, such as distal radius or metacarpal bone, has been reported to be selectively decreased compared with sites high in cancellous bone such as lumbar spine or femoral neck (21–24). Reduced GLP-1 secretion is one of the features of type 2 diabetes (9), and it is of interest that cortical bone loss is observed in Glp-1r$^{-/-}$ mice as well as in diabetic patients. Therefore, we suppose that modulation of GLP-1 receptor signaling may theoretically contribute to regulation of bone turnover in diabetic subjects, a hypothesis that requires further testing.

We found by bone histomorphometry that genetic loss of GLP-1 receptor signaling resulted in significantly increased osteoclastic bone resorption activity, whereas the effects on bone formation parameters were less marked, similar to the changes in bone turnover induced by gastrointestinal factors. However, unlike GIP, GLP-1 had no direct effects on osteoclasts and osteoblasts as shown by the *in vitro* experiments.

Calcitonin is a known inhibitor of bone resorption and has been reported to prevent or retard bone loss in animal models of excessive bone resorption (25–28). As to the effect of calcitonin on cortical bone, calcitonin treatment has been shown to increase lumbar vertebral cortical thickness (29) and femoral cortical areas (30) in ovariectomized rats. It has been reported that the GLP-1 receptor is expressed in thyroid C cells and that GLP-1 stimulates calcitonin secretion via a cAMP-mediated mechanism in cultured C cells (10, 11); we also found that GLP-1 has a stimulatory effect on calcitonin gene expression in thyroid C cells *in vivo*, because attempts at measurement of plasma calcitonin were not successful due to sample volumes and assay sensitivity. Thus, increased osteoclastic bone resorption in Glp-1r$^{-/-}$ mice might arise indirectly from loss of GLP-1 receptor signaling on C cells, leading to calcitonin deficiency. Consistent with this hypothesis, Glp-1r$^{-/-}$ mice exhibit reduced levels of calcitonin mRNA transcripts in the thyroid. Furthermore, calcitonin treatment effectively suppressed the urinary DPD concentration in Glp-1r$^{-/-}$ mice. Taken together, these findings are consistent with an essential role for calcitonin in the regulation of bone turnover (31) and raise the possibility that modulation of GLP-1 receptor signaling may regulate bone resorption indirectly through the thyroid C cell.

In summary, our present findings demonstrate that genetic disruption of GLP-1 receptor signaling results in cortical osteopenia and bone fragility due to increased bone resorption by osteoclasts, in association with reduced thyroid calcitonin expression. Moreover, exogenous GLP-1 administration increased calcitonin expression in the thyroid glands of normal WT mice. These findings raise the possibility that clinical modulation of GLP-1 receptor signaling in human subjects, either through administration of GLP-1 receptor agonists or dipeptidyl peptidase-4 inhibitors, may indirectly regulate bone turnover in diabetic subjects. Given the recent observations of reduced bone density and increased fracture rates in diabetic subjects treated with thiazolidinediones (32, 33), more studies directed at understanding the actions of therapies that activate GLP-1 receptor signaling seem warranted.

Acknowledgments

We gratefully acknowledge Ms. Akemi Ito, Niigata Bone Science Institute, for the measurement of bone histomorphometry, and also Dr. H. Yamauchi, Japan Osteoporosis Foundation, for technical advice on calcitonin experiments.

Received September 19, 2007. Accepted November 9, 2007.

Address all correspondence and requests for reprints to: Yuichiro Yamada, M.D., Ph.D., Department of Internal Medicine, Division of Endocrinology, Diabetes, and Geriatric Medicine, Akita University School of Medicine, 1-1-1 Hondo, Akita City, Akita 010-8543, Japan. E-mail: yamada@gipc.akita-u.ac.jp.

This work was supported by Grants-in-Aid for Scientific Research from the Ministry of Education, Culture, Sports, Science, and Technology, Japan; by Health Sciences Research Grants for Comprehensive Research on Aging and Health from the Ministry of Health, Labor, and Welfare, Japan; and by an operating grant from the Juvenile Diabetes Research Foundation, Canada, to D.J.D.

Present address for K.T.: Anjo Kosei Hospital, Japan.

Disclosure Statement: The authors have nothing to disclose.

References

1. Henriksen DB, Alexandersen P, Bjarnason NH, Vilsboll T, Hartmann B, Henriksen EE, Byrjalsen I, Krarup T, Holst JJ, Christiansen C 2003 Role of gastrointestinal hormones in postprandial reduction of bone resorption. J Bone Miner Res 18:2180–2189
2. Tsukiyama K, Yamada Y, Yamada C, Harada N, Kawasaki Y, Ogura M, Bessho K, Li M, Amizuka N, Sato M, Udagawa N, Takahashi N, Tanaka K, Oiso Y, Seino Y 2006 Gastric inhibitory polypeptide as an endogenous factor

promoting new bone formation after food ingestion. Mol Endocrinol 20:1644–1651
3. **Bollag RJ, Zhong Q, Phillips P, Min L, Zhong L, Cameron R, Mulloy AL, Rasmussen H, Qin F, Ding KH, Isales CM** 2000 Osteoblast-derived cells express functional glucose-dependent insulinotropic peptide receptors. Endocrinology 141:1228–1235
4. **Zhong Q, Itokawa T, Sridhar S, Ding KH, Xie D, Kang B, Bollag WB, Bollag RJ, Hamrick M, Insogna K, Isales CM** 2007 Effects of glucose-dependent insulinotropic peptide on osteoclast function. Am J Physiol Endocrinol Metab 292:E543–E548
5. **Xie D, Cheng H, Hamrick M, Zhong Q, Ding KH, Correa D, Williams S, Mulloy A, Bollag W, Bollag RJ, Runner RR, McPherson JC, Insogna K, Isales CM** 2005 Glucose-dependent insulinotropic polypeptide receptor knockout mice have altered bone turnover. Bone 37:759–769
6. **Xie D, Zhong Q, Ding KH, Cheng H, Williams S, Correa D, Bollag WB, Bollag RJ, Insogna K, Troiano N, Coady C, Hamrick M, Isales CM** 2007 Glucose-dependent insulinotropic peptide-overexpressing transgenic mice have increased bone mass. Bone 40:1352–1360
7. **Henriksen DB, Alexandersen P, Byrjalsen I, Hartmann B, Bone HG, Christiansen C, Holst JJ** 2004 Reduction of nocturnal rise in bone resorption by subcutaneous GLP-2. Bone 34:140–147
8. **Henriksen DB, Alexandersen P, Hartmann B, Adrian CL, Byrjalsen I, Bone HG, Holst JJ, Christiansen C** 2007 Disassociation of bone resorption and formation by GLP-2: a 14-day study in healthy postmenopausal women. Bone 40:723–729
9. **Vilsboll T, Krarup T, Deacon CF, Madsbad S, Holst JJ** 2001 Reduced postprandial concentrations of intact biologically active glucagon-like peptide 1 in type 2 diabetic patients. Diabetes 50:609–613
10. **Crespel A, De Boisvilliers F, Gros L, Kervran A** 1996 Effects of glucagon and glucagon-like peptide-1 (7–36) amide on C cells from rat thyroid and medullary thyroid carcinoma CA-77 cell line. Endocrinology 137:3674–3680
11. **Lamari Y, Boissard C, Moukhtar MS, Jullienne A, Rosselin G, Garel JM** 1996 Expression of glucagon like peptide 1 receptor in a murine C cell line: regulation of calcitonin gene by glucagon like peptide 1. FEBS Lett 393:248–252
12. **Hansotia T, Baggio LL, Delmeire D, Hinke SA, Yamada Y, Tsukiyama K, Seino Y, Holst JJ, Schuit F, Drucker DJ** 2004 Double incretin receptor knockout (DIRKO) mice reveal an essential role for the enteroinsular axis in transducing the glucoregulatory actions of DPP-IV inhibitors. Diabetes 53:1326–1335
13. **Yamanouchi K, Yada E, Hozumi H, Ueno C, Nishihara M** 2004 Analyses of hind leg skeletons in human growth hormone transgenic rats. Exp Gerontol 39:1179–1188
14. **Parfitt AM, Drezner MK, Glorieux FH, Kanis JA, Malluche H, Meunier PJ, Ott SM, Recker RR** 1987 Bone histomorphometry: standardization of nomenclature, symbols, and units. Report of the ASBMR Histomorphometry Nomenclature Committee. J Bone Miner Res 2:595–610
15. **Udagawa N, Takahashi N, Yasuda H, Mizuno A, Itoh K, Ueno Y, Shinki T, Gillespie MT, Martin TJ, Higashio K, Suda T** 2000 Osteoprotegerin produced by osteoblasts is an important regulator in osteoclast development and function. Endocrinology 141:3478–3484
16. **Li X, Udagawa N, Itoh K, Suda K, Murase Y, Nishihara T, Suda T, Takahashi N** 2002 p38 MAPK-mediated signals are required for inducing osteoclast differentiation but not for osteoclast function. Endocrinology 143:3105–3113
17. **Schwartz AV** 2003 Diabetes mellitus: does it affect bone? Calcif Tissue Int 73:515–519
18. **Carnevale V, Romagnoli E, D'Erasmo E** 2004 Skeletal involvement in patients with diabetes mellitus. Diabetes Metab Res Rev 20:196–204
19. **Rakic V, Davis WA, Chubb SA, Islam FM, Prince RL, Davis TM** 2006 Bone mineral density and its determinants in diabetes: the Fremantle Diabetes Study. Diabetologia 49:863–871
20. **Bagi CM, Hanson N, Andresen C, Pero R, Lariviere R, Turner CH, Laib A** 2006 The use of micro-CT to evaluate cortical bone geometry and strength in nude rats: correlation with mechanical testing, pQCT and DXA. Bone 38:136–144
21. **Christensen J O, Svendsen OL** 1999 Bone mineral in pre- and postmenopausal women with insulin-dependent and non-insulin-dependent diabetes mellitus. Osteoporos Int 10:307–311
22. **Suzuki K, Sugimoto C, Takizawa M, Ishizuka S, Kikuyama M, Togawa H, Taguchi Y, Nosaka K, Seino Y, Ishida H** 2000 Correlations between bone mineral density and circulating bone metabolic markers in diabetic patients. Diabetes Res Clin Pract 48:185–191
23. **Majima T, Komatsu Y, Yamada T, Koike Y, Shigemoto M, Takagi C, Hatanaka I, Nakao K** 2005 Decreased bone mineral density at the distal radius, but not at the lumbar spine or the femoral neck, in Japanese type 2 diabetic patients. Osteoporos Int 16:907–913
24. **Suzuki K, Kurose T, Takizawa M, Maruyama M, Ushikawa K, Kikuyama M, Sugimoto C, Seino Y, Nagamatsu S, Ishida H** 2005 Osteoclastic function is accelerated in male patients with type 2 diabetes mellitus: the preventive role of osteoclastogenesis inhibitory factor/osteoprotegerin (OCIF/OPG) on the decrease of bone mineral density. Diabetes Res Clin Pract 68:117–125
25. **Wronski TJ, Yen CF, Burton KW, Mehta RC, Newman PS, Soltis EE, DeLuca PP** 1991 Skeletal effects of calcitonin in ovariectomized rats. Endocrinology 129:2246–2250
26. **Li M, Shen Y, Burton KW, DeLuca PP, Mehta RC, Baumann BD, Wronski TJ** 1996 A comparison of the skeletal effects of intermittent and continuous administration of calcitonin in ovariectomized rats. Bone 18:375–380
27. **Wallach S, Rousseau G, Martin L, Azria M** 1999 Effects of calcitonin on animal and in vitro models of skeletal metabolism. Bone 25:509–516
28. **Mochizuki K, Inoue T** 2000 Effect of salmon calcitonin on experimental osteoporosis induced by ovariectomy and low-calcium diet in the rat. J Bone Miner Metab 18:194–207
29. **Mosekilde L, Danielsen CC, Gasser J** 1994 The effect on vertebral bone mass and strength of long term treatment with antiresorptive agents (estrogen and calcitonin), human parathyroid hormone (1–38), and combination therapy, assessed in aged ovariectomized rats. Endocrinology 134:2126–2134
30. **Giardino R, Fini M, Aldini NN, Gnudi S, Biagini G, Gandolfi MG, Mongiorgi R** 1996 Calcitonin and alendronate effects on bone quality in osteoporotic rats. J Bone Miner Res 21:S335 (Abstract)
31. **Huebner AK, Schinke T, Priemel M, Schilling S, Schilling AF, Emeson RB, Rueger JM, Amling M** 2006 Calcitonin deficiency in mice progressively results in high bone turnover. J Bone Miner Res 21:1924–1934
32. **Schwartz AV, Sellmeyer DE, Vittinghoff E, Palermo L, Lecka-Czernik B, Feingold KR, Strotmeyer ES, Resnick HE, Carbone L, Beamer BA, Park SW, Lane NE, Harris TB, Cummings SR** 2006 Thiazolidinedione use and bone loss in older diabetic adults. J Clin Endocrinol Metab 91:3349–3354
33. **Kahn SE, Haffner SM, Heise MA, Herman WH, Holman RR, Jones NP, Kravitz BG, Lachin JM, O'Neill MC, Zinman B, Viberti G** 2006 Glycemic durability of rosiglitazone, metformin, or glyburide monotherapy. N Engl J Med 355:2427–2443

Endocrinology **is published monthly by The Endocrine Society (http://www.endo-society.org), the foremost professional society serving the endocrine community.**

DIABETES RESEARCH AND CLINICAL PRACTICE XXX (2008) XXX–XXX

available at www.sciencedirect.com

ScienceDirect

journal homepage: www.elsevier.com/locate/diabres

Curcumin inhibits glucose production in isolated mice hepatocytes

Hideya Fujiwara [a], *Masaya Hosokawa* [a,*], *Xiaorong Zhou* [a], *Shimpei Fujimoto* [a], *Kazuhito Fukuda* [a], *Kentaro Toyoda* [a], *Yuichi Nishi* [a], *Yoshihito Fujita* [a], *Kotaro Yamada* [a], *Yuichiro Yamada* [a], *Yutaka Seino* [a,b], *Nobuya Inagaki* [a]

[a] *Department of Diabetes and Clinical Nutrition, Graduate School of Medicine, Kyoto University, 54 Shogoin, Kawahara-cho, Sakyo-ku, Kyoto 606-8507, Japan*

[b] *Kansai Denryoku Hospital, Osaka, Japan*

ARTICLE INFO

Article history:
Received 18 October 2007
Accepted 6 December 2007

Keywords:
Curcumin
Diabetes mellitus
Liver
Mice

ABSTRACT

Curcumin is a compound derived from the spice turmeric, and is a potent anti-oxidant, anti-carcinogenic, and anti-hepatotoxic agent. We have investigated the acute effects of curcumin on hepatic glucose production. Gluconeogenesis and glycogenolysis in isolated hepatocytes, and gluconeogenetic enzyme activity after 120 min exposure to curcumin were measured. Hepatic gluconeogenesis from 1 mM pyruvate was inhibited in a concentration-dependent manner, with a maximal decrease of 45% at the concentration of 25 μM. After 120 min exposure to 25 μM curcumin, hepatic gluconeogenesis from 2 mM dihydroxyacetone phosphate and hepatic glycogenolysis were inhibited by 35% and 20%, respectively. Insulin also inhibited hepatic gluconeogenesis from 1 mM pyruvate and inhibited hepatic glycogenolysis in a concentration-dependent manner. Curcumin (25 μM) showed an additive inhibitory effect with insulin on both hepatic gluconeogenesis and glycogenolysis, indicating that curcumin inhibits hepatic glucose production in an insulin-independent manner. After 120 min exposure to 25 μM curcumin, hepatic glucose-6-phosphatase (G6Pase) activity and phosphoenolpyruvate carboxykinase (PEPCK) activity both were inhibited by 30%, but fructose-1,6-bisphosphatase (FBPase) was not reduced. After 120 min exposure to 25 μM curcumin, phosphorylation of AMP kinase α-Thr^{172} was increased. Thus, the anti-diabetic effects of curcumin are partly due to a reduction in hepatic glucose production caused by activation of AMP kinase and inhibition of G6Pase activity and PEPCK activity.

1. Introduction

Curcumin is the major yellow pigment extracted from turmeric, the powdered rhizome of the herb *curcuma longa*. Turmeric is a spice used extensively in curries and mustards as a coloring and flavoring agent. Curcumin is reported to have a wide range of effects: it is anti-inflammatory [1], anti-oxidant [2,3] anti-hepatotoxic [4], and hypocholesterolemic [5,6]. Curcumin also is reported to have a beneficial effect on blood glucose in diabetic rats [7,8]. However, while elevated hepatic glucose production is

* *Corresponding author*. Tel.: +81 75 751 3560; fax: +81 75 751 4244.
E-mail address: hosokawa@metab.kuhp.kyoto-u.ac.jp (M. Hosokawa).

Abbreviations: DHAP, dihydroxyacetone phosphate; FBP, fructose-1,6-bisphophatase; G6Pase, glucose-6-phosphatase; PEPCK, phosphoenolpyruvate carboxykinase; AMP kinase, adenosine monophosphate activated protein kinase.

0168-8227/$ – see front matter © 2007 Elsevier Ireland Ltd. All rights reserved.
doi:10.1016/j.diabres.2007.12.004

Please cite this article in press as: H. Fujiwara et al., Curcumin inhibits glucose production in isolated mice hepatocytes, Diab. Res. Clin. Pract. (2008), doi:10.1016/j.diabres.2007.12.004

found frequently in type 2 diabetes, it is not known whether curcumin affects glucose metabolism in the liver. In the present study, we demonstrate that curcumin suppresses hepatic glucose production in an insulin-independent manner in isolated hepatocytes. We also investigated the inhibitory effect of curcumin on the activity of gluconeogenetic enzymes in isolated hepatocytes. Our results show that curcumin activates AMP kinase and suppresses both hepatic glucose-6-phosphatase (G6Pase) and phosphoenolpyruvate carboxykinase (PEPCK), thus inhibiting hepatic glucose output.

2. Materials and methods

2.1. Animals

C57/BL6J mice were purchased from Shimizu (Kyoto, Japan). The mice were allowed access to food, standard rat chow (Oriental Yeast, Osaka, Japan), and water *ad lib*. The mice were housed in an air-controlled (temperature 25 ± 2 °C and 50% humidity) room with a 12 h light/dark-cycle. For gluconeogenesis measurements, the mice were fasted 24 h with free access to water before the experiment. For glycogenolysis measurements, the mice were allowed access to food and water *ad lib* before the experiment.

2.2. Hepatocyte preparation

Liver of 10-week-old mice was perfused through the inferior *vena cava* with a buffer consisting of 140 mM NaCl, 2.6 mM KCl, 0.28 mM Na_2HPO_4, 5 mM glucose, and 10 mM Hepes (pH 7.4) after pentobarbital sodium anesthesia as described previously in Refs. [9,10]. The perfusion was first for 5 min with the buffer supplemented with 0.1 mM EGTA and then for 15 min with the buffer containing 5 mM $CaCl_2$ and 0.2 mg/ml collagenase type 2 (Worthington, Lakewood, NJ). All of the solutions were prewarmed at 37 °C and gassed with a mixture of 95% O_2/5%CO_2, resulting in pH 7.4. The isolated hepatocytes were filtered with nylon mesh (0.75 mm in diameter) and washed twice with the buffer above without collagenase, and suspended in a small volume of DMEM (GIBCO, Rockville, MD) without glucose or pyruvate, and counted. The viability of hepatocytes was evaluated by trypan blue staining. Samples with viability of less than 90% were discarded.

2.3. Hepatic glucose production

For gluconeogenesis measurements, hepatocytes (7.5×10^5) were incubated at 37 °C in a humidified atmosphere (5% CO_2) in 0.5 ml of DMEM without glucose but containing 1 mM pyruvate or 2 mM dihydroxyacetone phosphate (DHAP), 0.24 mM 3-isobutyl-1-methylxanthine in the presence or absence of curcumin or insulin. For glycogenolysis measurements, hepatocytes (7.5×10^5) were incubated at 37 °C in a humidified atmosphere (5% CO_2) in 0.5 ml of DMEM without glucose or pyruvate but containing 0.24 mM 3-isobutyl-1-methylxanthine in the presence or absence of curcumin or insulin. Curcumin was dissolved in DMSO to a concentration in the medium that did not interfere with cell viability (maximally 0.1%, v/v). Incubation was stopped by placing the cells on ice, followed by centrifugation at 4 °C for 60 s at 600 × *g*. The sampling was done at 0, 30, 60, and 120 min. The supernatant was removed, the cells were lysed in 0.1% of SDS in phosphate buffered saline, and the protein content was determined (BCA kit, Pierce). The glucose content of the supernatant was measured by glucose oxidation method (100 Trinder kit, Sigma). The dose–response of curcumin in gluconeogenesis and glycogenolysis were obtained at the incubation time of 120 min.

2.4. DNA synthesis measurement

DNA synthesis of hepatocytes was determined as the uptake of 5-bromo-2′-deoxyuridine (BrdU) according to the instruction manual (Cell Proliferation ELISA, BrdU (colorimetric), Roche Diagnostics, Manheim, Germany). After a 24-h preincubation of isolated hepatocytes with curcumin (25 μM) or vehicle in DMEM without glucose but with 10% fetal calf serum, hepatocytes were incubated for an additional 2 h with BrdU. The hepatocytes were fixed, and BrdU incorporation into DNA in hepatocytes was detected by ELISA. The results of incorporation of BrdU were expressed as photo-absorbance (wavelength 370–492 nm).

2.5. Enzyme activities

Hepatocytes were incubated at 37 °C in a humidified atmosphere (5% CO_2) in DMEM without glucose but containing 1 mM pyruvate and 0.24 mM 3-isobutyl-1-methylxanthine in the presence of 25 μM curcumin or vehicle (DMSO) for 120 min. Incubation was stopped by placing the cells on ice followed by centrifugation at 4 °C for 60 s at 600 × *g*. The supernatant was removed, and the cells were homogenized using a glass/Teflon homogenizer. In the microsomal preparation for the G6Pase assay, 50 mM Tris–HCl, pH 7.5, containing 250 mM sucrose, and 0.2 mM EDTA, was used as the homogenizing buffer [11]. For assay of G6Pase, liver microsomal fraction was prepared as follows: homogenate obtained as above was centrifuged at 20,000 × *g* for 20 min at 4 °C, and was then ultracentrifuged at 105,000 × *g* for 1 h at 4 °C. The resulting sediments were used for G6Pase assay [11]. The G6Pase activity was measured with intact microsomal preparation. Activity of G6Pase was determined as described by Passonneau and Lowry [12].

For liver PEPCK and fructose-1,6-bisphophatase (FBPase) assays, the homogenizing buffer contained 0.1 M Tris–HCl, pH 7.5, 0.15 M KCl, 5 mM EDTA, 5 mM dithiothreitol, and 5 mM $MgSO_4$ [11]. The homogenate was centrifuged at 105,000 × *g* for 1 h at 4 °C, and the supernatant was collected. Activity of FBPase was determined as described by Passonneau and Lowry [12].

Activity of PEPCK was determined as described by Nakagawa and Nagai [13]. All enzyme activity was measured photometrically using BIO-RAD Benchmark Plus.

Enzyme activities are expressed as the number of substrate molecules converted by 1 mg cytosolic or microsomal protein per minute. The liver microsomal fraction was solubilized by addition of 0.1% SDS before protein determination.

2.6. Immunoblotting analysis

Hepatocytes were incubated at 37 °C in a humidified atmosphere (5% CO_2) in 10 ml of DMEM without glucose but

Please cite this article in press as: H. Fujiwara et al., Curcumin inhibits glucose production in isolated mice hepatocytes, Diab. Res. Clin. Pract. (2008), doi:10.1016/j.diabres.2007.12.004

containing 1 mM pyruvate and 0.24 mM 3-isobutyl-1-methylxanthine in the presence of 25 μM curcumin or vehicle (DMSO) for 120 min. Incubation was stopped by placing the cells on ice followed by centrifugation at 4 °C for 60 s at 600 × *g*. The supernatant was removed, and the cells were homogenized in ice-cold lysis buffer (50 mM Tris–HCl, pH 7.4, 50 mM NaF, 1 mM sodium pyrophosphate, 1 mM EDTA, 1 mM EGTA, 1 mM dithiothreitol, 0.1 mM benzamidine, 0.1 mM phenylmethylsulfonylfluoride, 0.2 mM sodium vanadate, 250 mM mannitol, 1% Triton X-100, and 5 μg/ml soybean trypsin inhibitor). The cell lysates were sonicated twice for 10 s and centrifuged at 13,000 × *g* for 5 min. The pellets were discarded, and supernatants were assayed for protein concentration. Equal amounts of proteins (50 μg) were subjected to SDS-polyacrylamide (8%) gel electrophoresis and transferred onto nitrocellulose membranes (PROTRAN, Schleicher & Schuell) by electroblotting. After pre-incubation with blocking buffer (PBS containing 0.1% Tween 20 and 5% nonfat dry milk) for 2 h at room temperature, blotted membranes were incubated with each primary antibody (phospho-AMP kinase α-Thr^{172} antibody or AMP kinase α antibody, Cell Signaling Technology, Danvers, MA) overnight at 4 °C, followed by washing twice with blocking buffer. Membranes were then incubated with a horseradish peroxidase-linked anti-rabbit IgG (Amersham) for 1 h at room temperature, washed twice in PBS containing 0.04% Tween 20, and visualized by ECL Western blotting detection reagents (Amersham). Densitometry was carried out to measure band intensities and phosphorylated AMP kinase α-Thr^{172} was normalized by the levels of AMP kinase α protein.

2.7. Materials

Curcumin was purchased from Wako Chemicals (Osaka, Japan). Standard rat chow was from Oriental Yeast (Osaka, Japan). Human insulin was from Novo-Nordisk (Copenhagen, Denmark). All other chemicals were of reagent grade.

2.8. Statistical analysis

Results are mean ± S.E.M. (*n* = number of animals). Statistical significance was evaluated using two-tailed Student's t-tests. Differences among groups were also statistically examined by one-way ANOVA (Fisher's PLSD test). $P < 0.05$ was considered significant.

2.9. Ethical considerations

All studies were performed in the laboratories of the Department of Diabetes and Clinical Nutrition, Kyoto University, in accordance with the Declaration of Helsinki.

3. Results

3.1. Effect of curcumin on hepatic gluconeogenesis in freshly isolated hepatocytes

Fig. 1A shows the time course of inhibition by curcumin of hepatic gluconeogenesis from pyruvate. After 30, 60, and 120 min exposure to 25 μM curcumin, hepatic gluconeogenesis was significantly inhibited by approximately 45%, 40%, and 45%, respectively. The viability of the hepatocytes was not affected by 120 min exposure to 25 μM curcumin (control: 78 ± 1% vs. curcumin: 79 ± 2%). Fig. 1B shows the time course of inhibition by curcumin of hepatic gluconeogenesis from dihydroxyacetone phosphate. After 120 min exposure to 25 μM curcumin, hepatic gluconeogenesis was significantly inhibited by approximately 35%.

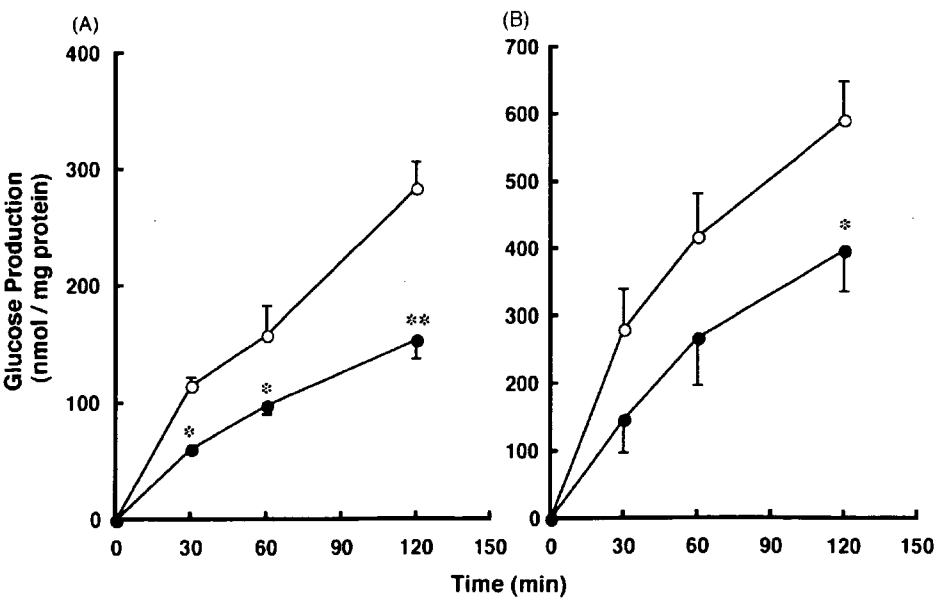

Fig. 1 – Time course of inhibition in hepatic gluconeogenesis from 1 mM pyruvate (A) and 2 mM DHAP (B). Isolated hepatocytes from fasted mice were incubated in the presence of 25 μM curcumin or vehicle for 2 h. Glucose content in supernatant was measured by glucose oxidation method. Each point shows mean ± S.E.M. (*n* = 6). *$P < 0.05$, **$P < 0.01$ compared with control by unpaired Student's t-test. Control (○), curcumin (●).

Please cite this article in press as: H. Fujiwara et al., Curcumin inhibits glucose production in isolated mice hepatocytes, Diab. Res. Clin. Pract. (2008), doi:10.1016/j.diabres.2007.12.004

As shown in Fig. 2, curcumin inhibited hepatic gluconeogenesis from pyruvate at the incubation time of 120 min in a concentration-dependent manner.

As shown in Fig. 3, after 120 min exposure to insulin, hepatic gluconeogenesis from pyruvate was inhibited in a concentration-dependent manner. After 120 min exposure to various concentrations of insulin (0.1, 1, and 10 nM) in the presence of 25 μM curcumin, hepatic gluconeogenesis from pyruvate was further inhibited by approximately 45% when compared to that in the absence of 25 μM curcumin.

3.2. *Effect of curcumin on DNA synthesis in isolated hepatocytes*

To determine whether curcumin is toxic to hepatocytes, we examined the effect of curcumin on DNA synthesis in isolated hepatocytes. After 24 h exposure to 25 μM curcumin, BrdU incorporation into DNA in isolated hepatocytes was not decreased compared to control, indicating no suppressive effects of curcumin on DNA synthesis (Fig. 4).

3.3. *Effect of curcumin on hepatic glycogenolysis in freshly isolated hepatocytes*

Fig. 5A shows the time course of inhibition by curcumin of hepatic glucose production from glycogenolysis. After 60 and 120 min exposure to 25 μM curcumin, hepatic glycogenolysis was significantly inhibited by approximately 10% and 20%, respectively. As shown in Fig. 5B, curcumin inhibited hepatic glycogenolysis at the incubation time of 120 min in a concentration-dependent manner. As shown in Fig. 6, after

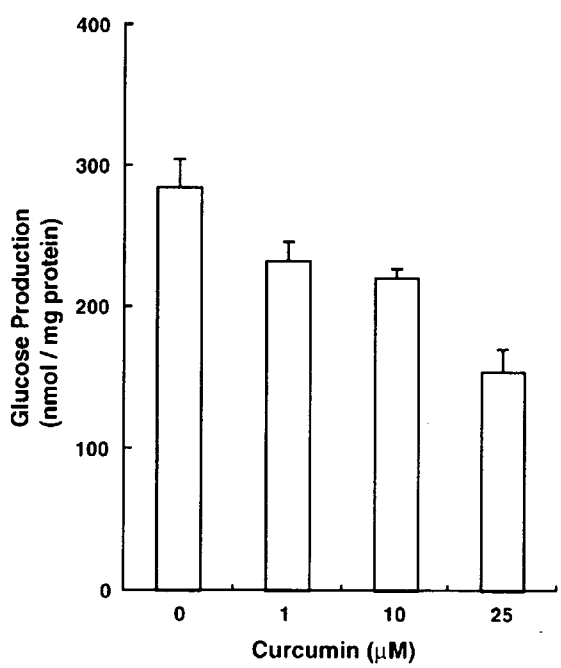

Fig. 2 – Concentration-dependence of inhibition in gluconeogenesis from 1 mM pyruvate by curcumin at the incubation time of 120 min in isolated mice hepatocytes. Each point shows mean ± S.E.M. ($n = 6$). $P < 0.001$ by one-way ANOVA.

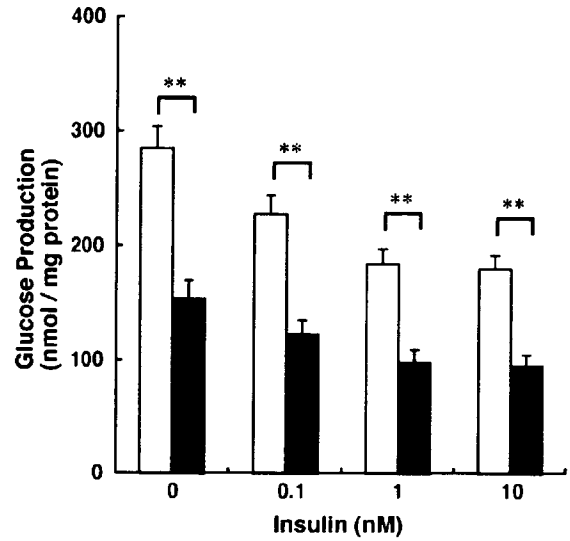

Fig. 3 – Concentration-dependence of inhibition in gluconeogenesis from 1 mM pyruvate by insulin in the presence and absence of 25 μM curcumin in isolated mice hepatocytes. Each point shows mean ± S.E.M. ($n = 6$). $P < 0.001$ by one-way ANOVA. **$P < 0.01$ compared with insulin alone by unpaired Student's t-test. Insulin alone (open bar), insulin plus curcumin (closed bar).

120 min exposure to insulin, hepatic glycogenolysis was inhibited in a concentration-dependent manner. After 120 min exposure to various concentrations of insulin (0.1, 1, and 10 nM) in the presence of 25 μM curcumin, hepatic glycogenolysis was further inhibited by approximately 20% compared to that in the absence of 25 μM curcumin.

3.4. *Effect of curcumin on activities of hepatic gluconeogenetic enzymes*

To further investigate inhibition of hepatic glucose production by curcumin, we measured the activities of key gluconeogenetic enzymes, G6Pase, FBPase, and PEPCK. After 120 min exposure to 25 μM curcumin, hepatic G6Pase activity and PEPCK activity were significantly inhibited by approximately 30%, but FBPase was not inhibited (Fig. 7).

3.5. *Effect of curcumin on phosphorylation of AMP kinase*

AMP kinase activation was monitored in Western blots by staining with a specific antibody against phosphorylated Thr^{172} of AMP kinase α, which is essential for AMP kinase activity. After 120 min exposure to 25 μM curcumin, phosphorylation of AMP kinase α-Thr^{172} was significantly increased by 70% when normalized by total content of AMP kinase α, clearly indicating curcumin activation of AMP kinase (Fig. 8).

4. Discussion

This is the first study to show that curcumin reduces hepatic glucose production. Our results demonstrate that curcumin

Please cite this article in press as: H. Fujiwara et al., Curcumin inhibits glucose production in isolated mice hepatocytes, Diab. Res. Clin. Pract. (2008), doi:10.1016/j.diabres.2007.12.004

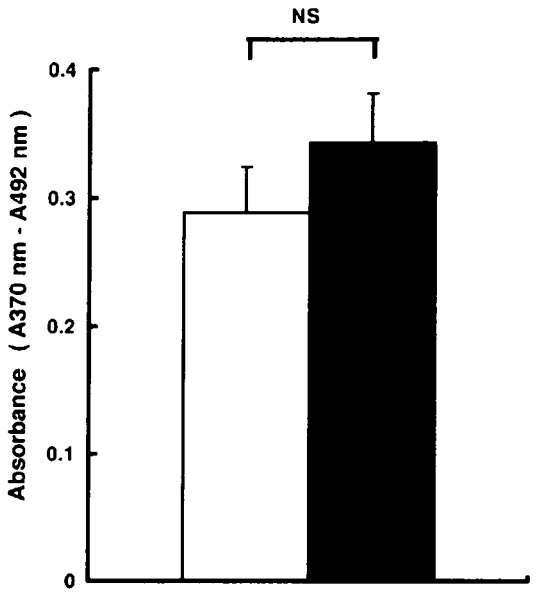

Fig. 4 – The effect of curcumin on DNA synthesis in isolated hepatocytes. After 24-h pre-incubation of isolated mice hepatocytes with 25 μM curcumin or vehicle in DMEM without glucose but with 10% fetal calf serum, hepatocytes were incubated for an additional 2 h with BrdU. The results of incorporation of BrdU were expressed as photo-absorbance (wavelength 370–492 nm). Control (open bar), curcumin (closed bar).

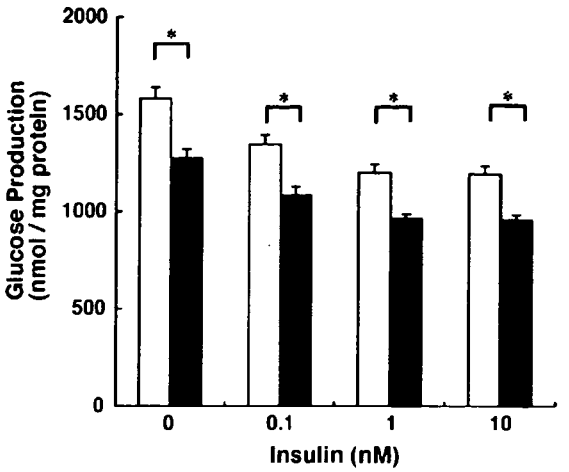

Fig. 6 – Concentration-dependence of inhibition in glycogenolysis by insulin in the presence and absence of 25 μM curcumin at the incubation time of 120 min in isolated mice hepatocytes. Each point shows mean ± S.E.M. ($n = 6$). $P < 0.001$ by one-way ANOVA. *$P < 0.05$ compared with insulin alone by unpaired Student's t-test. Insulin alone (open bar), insulin plus curcumin (closed bar).

inhibits both hepatic gluconeogenesis and glycogenolysis by suppressing both G6Pase activity and PEPCK activity. As curcumin had no suppressive effect on DNA synthesis in isolated hepatocytes, the inhibition of hepatic glucose production should not be a toxic effect. Indeed, Shen et al.

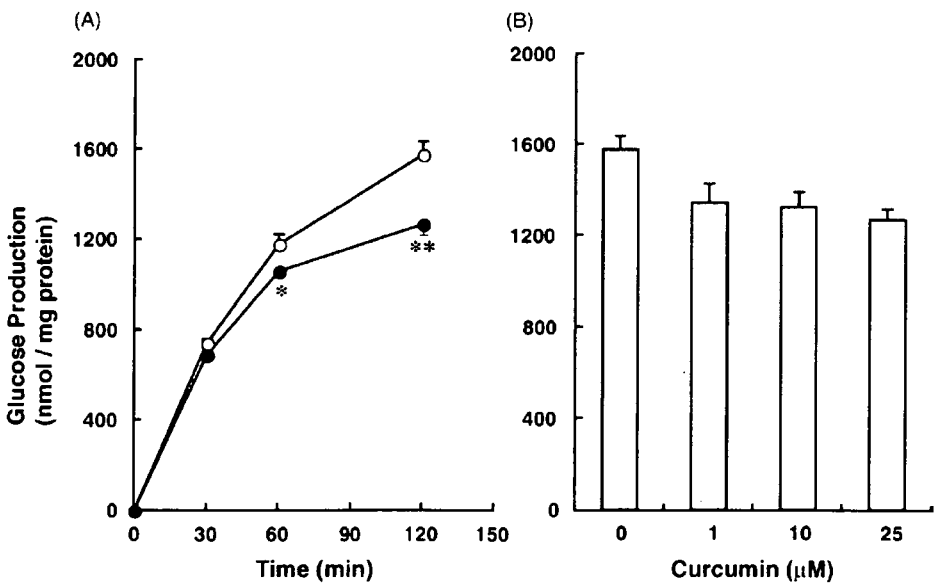

Fig. 5 – (A) Time course of inhibition of hepatic glucose production from glycogenolysis by curcumin. Isolated hepatocytes from fed mice were incubated in the presence of 25 μM curcumin or vehicle for 2 h. Glucose content in supernatant was measured by glucose oxidation method. Each point shows mean ± S.E.M. ($n = 5$). *$P < 0.05$, **$P < 0.01$ compared with control by unpaired Student's t-test. Control (○), curcumin (●). (B) Concentration-dependence of inhibition of glycogenolysis by curcumin at the incubation time of 120 min in isolated mice hepatocytes. Each point shows mean ± S.E.M. ($n = 6$). $P < 0.05$ by one-way ANOVA.

Please cite this article in press as: H. Fujiwara et al., Curcumin inhibits glucose production in isolated mice hepatocytes, Diab. Res. Clin. Pract. (2008), doi:10.1016/j.diabres.2007.12.004

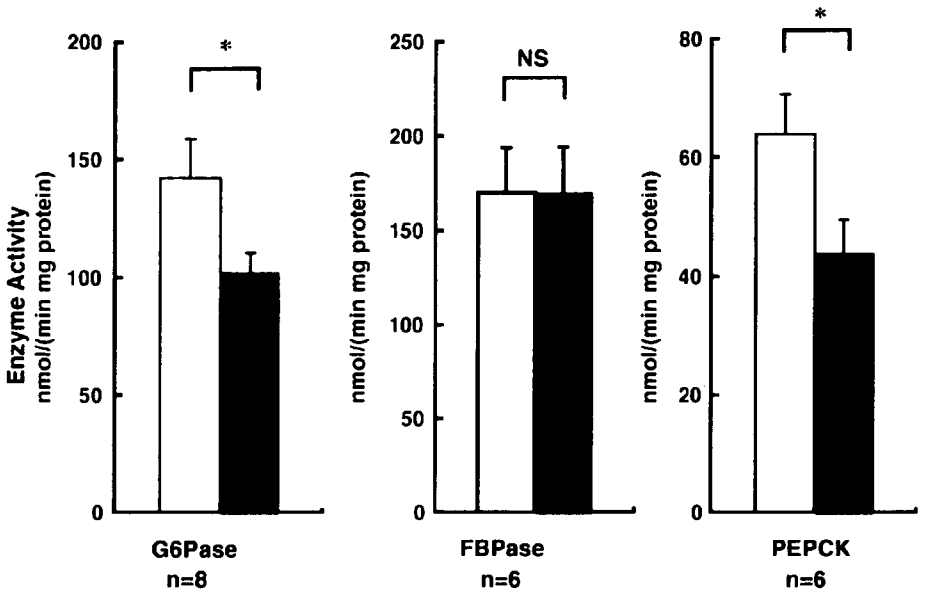

Fig. 7 – Effects of curcumin on hepatic gluconeogenetic activities of G6Pase, FBPase, and PEPCK in isolated mice hepatocyte. Isolated hepatocytes from fasted mice were incubated in the presence of 25 μM curcumin or vehicle for 2 h. All enzyme activities were measured photometrically. Enzyme activities are expressed as the number of substrate molecules converted by 1 mg cytosolic or microsomal protein per minute. Each point shows mean ± S.E.M. *P < 0.05 compared with control by unpaired Student's t-test. Control (open bar), curcumin (closed bar).

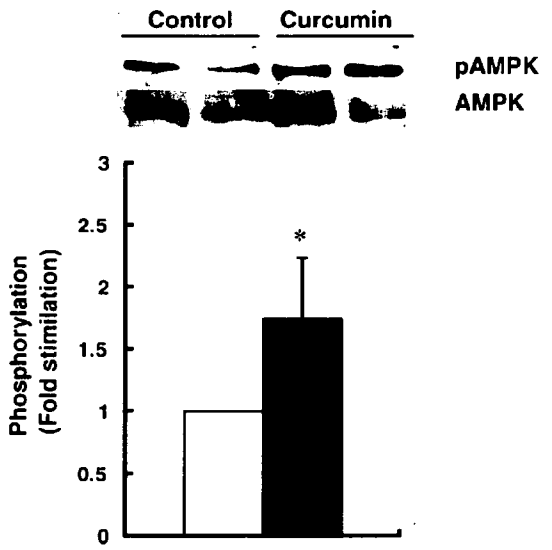

Fig. 8 – Effect of curcumin on activation of AMP kinase in isolated mice hepatocytes. AMP kinase activation was monitored in Western blots by staining with a specific antibody against phosphorylated Thr^{172} of AMP kinase α. After 120 min exposure to 25 μM curcumin, the level of phosphorylation of AMP kinase α-Thr^{172} (pAMPK) was significantly increased by 70% when normalized by total content of AMP kinase α (AMPK), and is expressed as fold stimulation over the control (mean ± S.E.M., n = 5) (lower panel). Upper panel shows a representative immunoblot of pAMPK and AMPK in hepatocytes from two mice in each group. *P < 0.05 compared with control by unpaired Student's t-test. Control (open bar), curcumin (closed bar).

recently reported a protective effect of curcumin against warm ischemia/reperfusion injury in rat liver [14].

Arun and Nalini reported that curcumin reduced blood glucose in alloxan-induced diabetic rats [7], but the mechanism of the anti-diabetic action was left unclear in that study. In the present study, insulin was found to dose-dependently inhibit hepatic gluconeogenesis, reaching a plateau at a concentration of 10 nM. In the presence of 10 nM insulin, the addition of 25 μM curcumin enchanced the inhibitory effect of insulin on hepatic gluconeogenesis, demonstrating that curcumin inhibits hepatic gluconeogenesis by a pathway independent of insulin signaling. Thus, curcumin is an insulin-sentitizing agent.

Recently, the major effect of metformin, a biguanide, was reported to be inhibition of hepatic G6Pase activity and hepatic glucose production in rats fed a high-fat diet [15]. Zhou et al. reported that metformin activated AMP kinase in hepatocytes [16]. The activation of AMP kinase is known to suppress gene expression of G6Pase and PEPCK and to inhibit hepatic glucose production in an insulin-independent manner [17,18]. In the present study, curcumin was found to inhibit both G6Pase and PEPCK activity; we therefore measured the effect of curcumin on AMP kinase activity to clarify the underlying mechanism. Zang et al. reported that resveratrol, a polyphenol and an anti-oxidant, which is a key component in red wine, stimulates AMP kinase in hepatoma HepG2 cells [19]. Kim et al. reported that cryptotanshinone, another anti-oxidant and a diterpene, which was originally isolated from dried roots of *Salvia mlitorrhiza* Bunge, showed anti-diabetic effects through activation of AMP kinase [20]. Considering these findings together, the potent anti-oxidant effect of curcumin may

Please cite this article in press as: H. Fujiwara et al., Curcumin inhibits glucose production in isolated mice hepatocytes, Diab. Res. Clin. Pract. (2008), doi:10.1016/j.diabres.2007.12.004

well be involved in the activation of AMP kinase. Further investigation is required to clarify the anti-diabetic action of curcumin in hepatocytes.

Biguanide sometimes shows the lethal adverse effect of lactic acidosis in diabetic patients when prescribed inappropriately. On the other hand, since curcumin is derived from an extensively used dietary spice, the compound may well be safely administered to humans. Indeed, Sharma et al. administered oral daily curcumin to advanced colorectal cancer patients without major adverse effects [21]. Cheng et al. also administered oral daily curcumin to patients with high risk or pre-malignant lesions [22].

Considered together with our results, these data suggest that curcumin might provide a valuable new therapy in the treatment of type 2 diabetes.

Acknowledgements

This study was supported in part by Grants-in-Aids for Scientific Research from the Ministry of Education, Culture, Sports, Science and Technology of Japan; Health and Labour Sciences Research Grants for Research on Human Genome, Tissue Engineering, and Food Biotechnology from the Ministry of Health, Labor and Welfare of Japan; and Health and Labour Sciences Research Grants for Comprehensive Research on Aging and Health from the Ministry of Health, Labor and Welfare of Japan.

Conflict of interest

The authors state that they have no conflict of interest.

REFERENCES

[1] R.C. Srimal, B.N. Dhawan, Pharmacology of diferuloyl methane (curcumin), a non-steroidal anti-inflammatory agent, J. Pharm. Pharmacol. 25 (1973) 447–452.

[2] B. Joe, B.R. Lokesh, Role of capsaicin, curcumin and dietary n-3 fatty acids in lowering the generation of reactive oxygen species in rat peritoneal macrophages, Biochim. Biophys. Acta 1224 (1994) 255–263.

[3] A.C. Reddy, B.R. Lokesh, Studies on the inhibitory effects of curcumin and eugenol on the formation of reactive oxygen species and the oxidation of ferrous iron, Mol. Cell. Biochem. 137 (1994) 1–8.

[4] Y. Kiso, Y. Suzuki, N. Watanabe, Y. Oshima, H. Hikino, Antihepatotoxic principles of *Curcuma longa* rhizomes, Planta Med. 49 (1983) 185–187.

[5] D.S. Rao, N.C. Sekhara, M.N. Satyanarayana, M. Srinivasan, Effect of curcumin on serum and liver cholesterol levels in the rat, J. Nutr. 100 (1970) 1307–1315.

[6] T.N. Patil, M. Srinivasan, Hypocholesteremic effect of curcumin in induced hypercholesteremic rats, Indian J. Exp. Biol. 9 (1971) 167–169.

[7] N. Arun, N. Nalini, Efficacy of turmeric on blood sugar and polyol pathway in diabetic albino rats, Plant Foods Hum. Nutr. 57 (2002) 41–52.

[8] T. Nishiyama, T. Mae, H. Kishida, M. Tsukagawa, Y. Mimaki, M. Kuroda, et al., Curcuminoids and sesquiterpenoids in turmeric (*Curcuma longa* L.) suppress an increase in blood glucose level in type 2 diabetic KK-Ay mice, J. Agric. Food Chem. 53 (2005) 959–963.

[9] M. Hosokawa, B. Thorens, Glucose release from GLUT2-null hepatocytes: characterization of a major and a minor pathway, Am. J. Physiol. Endocrinol. Metab. 282 (2002) E794–E801.

[10] M. Uldry, M. Ibberson, M. Hosokawa, B. Thorens, GLUT2 is a high affinity glucosamine transporter, FEBS Lett. 524 (2002) 199–203.

[11] K. Aoki, T. Saito, S. Satoh, K. Mukasa, M. Kaneshiro, S. Kawasaki, et al., Dehydroepiandrosterone suppresses the elevated hepatic glucose-6-phosphatase and fructose-1,6-bisphosphatase activities in C57BL/Ksj-db/db mice: comparison with troglitazone, Diabetes 48 (1999) 1579–1585.

[12] J.V. Passoneau, O.H. Lowry, Enzymic Analysis: A Practical Guide by Passoneau JV and Lowry OH., Humana Press, Totowa, NJ, 1993, pp. 249–253.

[13] H. Nakagawa, K. Nagai, Cold adaptation. I. Effect of cold-exposure on gluconeogenesis, J. Biochem. (Tokyo) 69 (1971) 923–934.

[14] S.Q. Shen, Y. Zhang, J.J. Xiang, C.L. Xiong, Protective effect of curcumin against liver warm ischemia/reperfusion injury in rat model is associated with regulation of heat shock protein and antioxidant enzymes, World J. Gastroenterol. 13 (2007) 1953–1961.

[15] G. Mithieux, L. Guignot, J.C. Bordet, N. Wiernsperger, Intrahepatic mechanisms underlying the effect of metformin in decreasing basal glucose production in rats fed a high-fat diet, Diabetes 51 (2002) 139–143.

[16] G. Zhou, R. Myers, Y. Li, Y. Chen, X. Shen, J. Fenyk-Melody, et al., Role of AMP-activated protein kinase in mechanism of metformin action, J. Clin. Invest. 108 (2001) 1167–1174.

[17] P.A. Lochhead, I.P. Salt, K.S. Walker, D.G. Hardie, C. Sutherland, 5-Aminoimidazole-4-carboxamide riboside mimics the effects of insulin on the expression of the 2 key gluconeogenic genes PEPCK and glucose-6-phosphatase, Diabetes 49 (2000) 896–903.

[18] T. Yamauchi, J. Kamon, Y. Minokoshi, Y. Ito, H. Waki, S. Uchida, et al., Adiponectin stimulates glucose utilization and fatty-acid oxidation by activating AMP-activated protein kinase, Nat. Med. 8 (2002) 1288–1295.

[19] M. Zang, S. Xu, K.A. Maitland-Toolan, A. Zuccollo, X. Hou, B. Jiang, et al., Polyphenols stimulate AMP-activated protein kinase, lower lipids, and inhibit accelerated atherosclerosis in diabetic LDL receptor-deficient mice, Diabetes 55 (2006) 2180–2191.

[20] E.J. Kim, S.N. Jung, K.H. Son, S.R. Kim, T.Y. Ha, M.G. Park, et al., Antidiabetes and antiobesity effect of cryptotanshinone via activation of AMP-activated protein kinase, Mol. Pharmacol. 72 (2007) 62–72.

[21] R.A. Sharma, S.A. Euden, S.L. Platton, D.N. Cooke, A. Shafayat, H.R. Hewitt, et al., Phase I clinical trial of oral curcumin: biomarkers of systemic activity and compliance, Clin. Cancer Res. 10 (2004) 6847–6854.

[22] A.L. Cheng, C.H. Hsu, J.K. Lin, M.M. Hsu, Y.F. Ho, T.S. Shen, et al., Phase I clinical trial of curcumin, a chemopreventive agent, in patients with high-risk or pre-malignant lesions, Anticancer Res. 21 (2001) 2895–2900.

Please cite this article in press as: H. Fujiwara et al., Curcumin inhibits glucose production in isolated mice hepatocytes, Diab. Res. Clin. Pract. (2008), doi:10.1016/j.diabres.2007.12.004

0013-7227/07/$15.00/0
Printed in U.S.A.

Endocrinology 148(11):5268–5277
Copyright © 2007 by The Endocrine Society
doi: 10.1210/en.2007-0349

Ceramide and Adenosine 5′-Monophosphate-Activated Protein Kinase Are Two Novel Regulators of 11β-Hydroxysteroid Dehydrogenase Type 1 Expression and Activity in Cultured Preadipocytes

N. Arai, H. Masuzaki, T. Tanaka, T. Ishii, S. Yasue, N. Kobayashi, T. Tomita, M. Noguchi, T. Kusakabe, J. Fujikura, K. Ebihara, M. Hirata, K. Hosoda, T. Hayashi, H. Sawai, Y. Minokoshi, and K. Nakao

Division of Endocrinology and Metabolism (N.A., H.M., T.Ta., T.I., S.Y., N.K., T.To., M.N., T.K., J.F., K.E., M.H., K.H., K.N.), Department of Medicine and Clinical Science, Kyoto University Graduate School of Medicine, Kyoto 606-8507, Japan; Department of Human Coexistence (T.H.), Kyoto University Graduate School of Human and Environmental Studies, Kyoto 606-8501, Japan; Department of Internal Medicine (H.S.), Osaka Dental University, Osaka 573-1121, Japan; and Department of Developmental Physiology (Y.M.), National Institute for Physiological Science, Aichi 444-8585, Japan

Increased activity of intracellular glucocorticoid reactivating enzyme, 11β-hydroxysteroid dehydrogenase type 1 (11β-HSD1) in obese adipose tissue contributes to adipose dysfunction. As recent studies have highlighted a potential role of preadipocytes in adipose dysfunction, we tested the hypothesis that a variety of metabolic stress mediated by ceramide or AMP-activated protein kinase (AMPK) would regulate 11β-HSD1 in preadipocytes. The present study is the first to show that 1) expression of 11β-HSD1 in 3T3-L1 preadipocytes was robustly induced when cells were treated with cell-permeable ceramide analogue C_2 ceramide, bacterial sphingomyelinase, and sphingosine 1-phosphate, 2) 5-aminoimidazole-4-carboxamide ribonucleoside (AICAR)-induced activation of AMPK augmented the expression and enzyme activity of 11β-HSD1, and 3) these results were reproduced in human preadipocytes. We demonstrate for the first time that C_2 ceramide and AICAR markedly induced the expression of CCAAT/enhancer-binding protein (C/EBP) β and its binding to 11β-HSD1 promoter. Transient knockdown of C/EBPβ protein by small interfering RNA markedly attenuated the expression of 11β-HSD1 induced by C_2 ceramide or AICAR. The present study provides novel evidence that ceramide- and AMPK-mediated signaling pathways augment the expression and activity of 11β-HSD1 in preadipocytes by way of C/EBPβ, thereby highlighting a novel, metabolic stress-related regulation of 11β-HSD1 in a cell-specific manner. (*Endocrinology* 148: 5268–5277, 2007)

METABOLIC SYNDROME IS characterized by a cluster of glucose intolerance, hypertension, and dyslipidemia on a basis of insulin resistance and excess in intraabdominal fat accumulation (1–3). Functional abnormalities of adipose tissue have been implicated in the pathophysiology of metabolic syndrome (2). A series of transgenic and knockout experiments in mouse models suggest that exaggerated reactivation of glucocorticoid in adipose tissue, mediated by enzyme 11β-hydroxysteroid dehydrogenase type 1 (11β-HSD1), contributes to dysfunction of adipose tissue (3–7). 11β-HSD1 is a bidirectional (oxo-reductase and dehydrogenase) enzyme (8), expressing abundantly in adipose tissue, liver, and central nervous system (9, 10). Notably, 11β-HSD1 mainly acts as an oxo-reductase *in vivo* and reactivates inactive cortisone into active cortisol (8). Transgenic mice overexpressing 11β-HSD1 in adipose tissue exemplified major phenotype of metabolic syndrome (3, 4), whereas systemic 11β-HSD1 knockout mice were protected against diabetes and dyslipidemia on a high-fat diet (5–7). These data suggest that an increased level of adipose 11β-HSD1 considerably contributes to metabolic derangement. Consistent with this notion, selective 11β-HSD1 inhibitors are shown to ameliorate diabetes, dyslipidemia, and arteriosclerosis in experimental murine models (11, 12).

Obese adipose tissue is subjected to multiple cellular stresses such as endoplasmic reticulum stress and oxidative stress (13). Local hypoxia, tissue dysnutrition, and resultant cell death are potentially linked to macrophage recruitment and local inflammation in adipose tissue (13, 14). Recent studies also highlight a complexity of preadipocytes in controlling adipose tissue function (15, 16). Nevertheless mature adipocytes are the major component of adipose tissue and predominant source of 11β-HSD1 (10, 17); a considerable amount of 11β-HSD1 expression is also detected in stromal-vascular cells from adipose tissue (17). The underlying mechanism whereby 11β-HSD1 is elevated in obese adipose tissue still remains obscure, and the regulation of 11β-HSD1 in preadipocytes has been poorly understood.

In this context, we hypothesized that a variety of metabolic stresses would regulate the expression of 11β-HSD1 in preadipocytes. The sphingolipid ceramide serves as a bioactive lipid mediator in response to a variety of metabolic stresses

First Published Online August 16, 2007

Abbreviations: ACC, Acetyl-CoA carboxylase; AICAR, 5-aminoimidazole-4-carboxamide ribonucleosides; AMPK, AMP-activated protein kinase; C/EBP, CCAAT/enhancer-binding protein; ChIP, chromatin immunoprecipitation; 11β-HSD1, 11β-hydroxysteroid dehydrogenase type 1; MCP-1, monocyte chemoattractant protein-1; Pref-1, preadipocyte factor-1; SMase, sphingomyelinase; S1P, sphingosine 1-phosphate; siRNA, small interfering RNA.

Endocrinology is published monthly by The Endocrine Society (http://www.endo-society.org), the foremost professional society serving the endocrine community.

including inflammation and oxidative stress (18). Ceramide is generated by *de novo* synthesis as well as hydrolysis of membrane sphingomyelin by sphingomyelinase (SMase) (18, 19). Ceramide and its metabolites, sphingosine and sphingosine 1-phosphate (S1P), mediate a variety of biological events such as apoptosis, cell growth, and the stress response (18, 19). In contrast, AMP-activated protein kinase (AMPK) is another mediator of metabolic stress that responds to the negative energy balance within cells (20–22). AMPK is activated by stresses that increase intracellular AMP level such as local hypoxia, glucose deprivation, and ischemia (21). Whereas the function of AMPK in liver and muscle has been well investigated, its role in adipose tissue still remains obscure (23, 24). In the present study, using murine 3T3-L1 preadipocytes and human preadipocytes, we investigated the effect of ceramide- and AMPK-mediated signaling pathways on the expression of 11β-HSD1.

Materials and Methods

Reagents and chemicals

5-Aminoimidazole-4-carboxamide ribonucleoside (AICAR) was obtained from Toronto Research Chemicals (Toronto, Canada). A selective AMPK inhibitor, Compound C, and C_2 ceramide (*N*-acetyl-sphingosine) were purchased from Carbiochem (San Diego, CA). Bacterial SMase and S1P were from Sigma Chemicals (St. Louis, MO). Antibodies against phospho (Ser 79) acetyl-CoA carboxylase (ACC), CCAAT/enhancer-binding protein (C/EBP) β, and β-actin were from Upstate Biotechnology (Lake Placid, NY), Affinity BioReagents Inc. (Golden, CO), and Sigma Chemicals.

Cell culture and treatment

3T3-L1 fibrobrasts (kindly provided from Dr. H. Green and Dr. M. Morikawa, Harvard Medical School, Boston, MA) were maintained in DMEM containing 10% (vol/vol) calf serum at 37 C in 10% CO_2. Human perirenal preadipocytes were purchased from Cambrex (Walkersville, MD) (25, 26) and maintained according to the manufacturer's instructions. For differentiation of 3T3-L1 preadipocytes into mature adipocytes, cells (2 d postconfluence) were incubated with DMEM containing 10% (vol/vol) fetal bovine serum, 0.5 mM 3-isobutyl-1-methylxanthine, 0.25 μM dexamethasone, and 1 μg/ml insulin for 2 d, followed by another 2-d incubation with DMEM containing FBS and insulin (27). Additional incubation with DMEM containing FBS for 4 d completes the differentiation. Compound C and C_2 ceramide were dissolved in DMSO and added to the media within 0.1% of volume. S1P was dissolved in water containing 0.4% BSA and added to the media within 1.0% of volume.

RNA preparation and quantitative real-time PCR

Total RNA was extracted from cultured cells using TRIzol Reagent (Invitrogen, Carlsbad, CA), and cDNA was then synthesized using iScript cDNA Synthesis Kit (Bio-Rad, Hercules, CA) according to the manufacturer's instructions. To determine the mRNA levels, probes and primers were employed as follows: probe (5′FAM-tccgagttcaaggcagcgagacactacc-TAMRA-3′), forward (5′-ccaggtcggaggaaggtctc-3′), and reverse (5′-ccagcaatgtagtgagcagagg-3′) for murine 11β-HSD1; probe (5′FAM-ccccactcacctgctgctactcattca-TAMRA-3′), forward (5′-ttggctcagccagatgca-3′), and reverse (5′-ccagcctactcattgggatca-3′) for murine monocyte chemoattractant protein-1 (MCP-1); probe (5′FAM-acattgtcagcctcgcagaatccatactg-TAMRA-3′), forward (5′-atgcgacccaccctgtgac-3′), and reverse (5′-gaccctcccagccaacatg-3′) for murine preadipocyte factor-1 (Pref-1); and probe (5′-cattgttgtcgtctcctctctggctggg-3′), forward (5′-ttgcccatgctgaagcagag-3′), and reverse (5′-gcaaccattggataagccactt-3′) for human 11β-HSD1. TaqMan PCR was performed using ABI Prism 7700 Sequence Detection System as instructed by the manufacturer (Applied Biosystems, Foster City, CA). Each value of mRNA level was normalized to that of 18S rRNA.

Western blot analysis

Cells were washed twice with ice-cold PBS, and harvested in lysis buffer [40 mM HEPES, 10 mM EDTA, 100 mM NaF, 10 mM sodium pyrophosphate, 1 mM Na_3VO_4, 0.1 mg/ml aprotinin, 1 mM PMSF, 50 nM okadaic acid, and 1% (vol/vol) Nonidet P-40 at pH 7.5]. For analysis of C/EBPβ, cells were harvested in lysis buffer [1% (wt/vol) SDS, 60 mM Tris-HCl, 1 mM Na_3VO_4, 0.1 mg/ml aprotinin, 1 mM PMSF and 50 nM okadaic acid at pH 6.8], and boiled at 100 C for 10 min. After centrifugation, supernatants were normalized for protein concentration via Bradford method and then equal amounts of protein were subjected to SDS-PAGE and immunoblot.

Measurement of AMPK activity

Activation of AMPK is assessed by the immunoblot of Thr172-phosphorylated AMPKα. Antibodies against AMPKα and phosphorylated (Thr172) AMPK (Cell Signaling Technology, Beverly, MA) can detect both α1 and α2 isoform of the catalytic subunit (28). In 3T3-L1 adipocytes, AMPK activity is largely attributable to the α1 isoform (29), and both α1 and α2 catalytic subunit isoforms are activated by AICAR (29). The phosphorylation at Thr172 parallels the degree of AMPK activation, thus making it possible to estimate the activity of both isoform complexes (28).

Measurement of 11β-HSD1 activity

Assays for 11β-HSD1 activity were performed by incubating viable cells with 250 nM corticosteroids with appropriate tritium-labeled tracer. In assays for oxo-reductase activity, cells were incubated in serum-free DMEM containing 250 nM cortisone that includes 6.4 μCi/ml tritium-labeled tracer [1,2-^{3}H]$_2$ cortisone (Muromachi Yakuhin LTD, Kyoto, Japan). In assays for dehydrogenase activity, cells were incubated in serum-free DMEM containing 250 nM cortisol with 6.4 μCi/ml tritium-labeled tracer [1,2,6,7-^{3}H]$_4$ cortisol (Muromachi Yakuhin LTD). After the incubation at 37 C for indicated time, corticosteroids were extracted by ethyl acetate, separated by thin-layer chromatography in chloroform: methanol (95:5), and quantified by autoradiography. As a control (indicated as ref.), serum-free DMEM with tritium-labeled cortisone or cortisol was incubated without cells.

Chromatin immunoprecipitation (ChIP) analysis

ChIP analysis was performed using an assay kit (Upstate Biotechnology) according to the manufacturer's protocol. Anti-C/EBPβ antibody used for immunoprecipitation is from Santa Cruz Biotechnology (Santa Cruz, CA). Forward primer (5′-ctggaagttgcctcttactc-3′) and reverse primer (5′-cctgtaggacacacgaagaa-3′) were used to amplify the DNA fragment between −170 and +71 (relative to the transcription start site) of mouse 11β-HSD1 genomic DNA, which contains two putative C/EBP binding sites (30).

RNA interference (RNAi)

Two Stealth RNAi for mouse C/EBPβ were obtained (Invitrogen). Each small interfering RNA (siRNA), termed RNAi154 and RNAi168, was designed as a 25-bp duplex oligoribonucleotide with a sense strand corresponding to nucleotides 154–173 or 168–192 of the reported mouse C/EBPβ coding sequence (GenBank accession no. NM009883), respectively. The Stealth RNAi negative control duplex (Invitrogen) was used as a control oligoribonucleotide. According to the manufacturer's protocol, 3T3-L1 preadipocytes were transfected with 10 nM siRNA in antibiotic-free medium using Lipofectamine RNAiMAX (Invitrogen). The transfected cells were cultured overnight and applied to the experiments.

Statistical analysis

The data are presented as means ± SEM from independent three or four experiments. Student's *t* test was used to compare the data when the variances of two groups were regarded equal (within 5%). When variances of two groups were apparently different, Welch's *t* test was used. Differences were accepted as significant at $P < 0.05$ level.

Results

When 3T3-L1 preadipocytes were differentiated into mature adipocytes, the level of 11β-HSD1 mRNA was increased by 150-fold (Fig. 1). Based on this result, we first analyzed the effect of ceramide signaling on the expression of 11β-HSD1 in both 3T3-L1 preadipocytes and differentiated adipocytes.

Effect of ceramide on the expression of 11β-HSD1 in 3T3-L1 preadipocytes

When 3T3-L1 preadipocytes were treated with a short chain ceramide analog, C_2 ceramide (10–100 μM), for 24 h, mRNA of Pref-1, which is known to express abundantly in preadipocytes (31, 32), was not altered (Fig. 2A). In contrast, expression of MCP-1 and 11β-HSD1 was induced dose-dependently, reaching to 2.0 ± 0.1-fold ($P < 0.01$) and 2.2 ± 0.1-fold ($P < 0.01$), respectively (Fig. 2, B and C). To evaluate the effect of C_2 ceramide on the 11β-HSD1 enzyme activity, cells were incubated with tritium-labeled cortisone or cortisol. C_2 ceramide significantly increased the conversion of cortisone to cortisol by 1.7 ± 0.1-fold ($P < 0.05$) (Fig. 2D, *left*). This indicates that 11β-HSD1 oxo-reductase activity was increased in response to C_2 ceramide. In contrast, 11β-HSD1 dehydrogenase activity was neither detected nor induced during a 24-h incubation period (Fig. 2D, *right*). These results indicate that 11β-HSD1 in 3T3-L1 preadipocytes acts solely as an oxo-reductase.

Hydrolysis of membrane sphingomyelin by SMase provoke intracellular accumulation of ceramide (19). Ceramide is subsequently metabolized to sphingosine and S1P, both of which mediate biological events including cell growth and apoptosis (19). We thus treated 3T3-L1 preadipocytes with bacterial SMase and S1P. When cells were treated with bacterial SMase (25–200 mU/ml) and S1P (1.0–10 μM), 11β-HSD1 mRNA level was significantly induced, reaching to 1.7 ± 0.2-fold ($P < 0.05$) and 3.0 ± 0.5-fold ($P < 0.05$), respectively (Fig. 2, E and F). To further investigate whether ceramide signaling would be involved in the induction of 11β-HSD1 by inflammatory cytokines, inhibitors of ceramide [fumonisin B1, an inhibitor of ceramide synthase (33); myriocin, an inhibitor of serine palmitoyltransferase (34); desipramine, an inhibitor of SMase (35)] were cotreated with 3T3-L1 preadipocytes. Desipramine (10 and 20 μM) dose-dependently attenuated the expression of 11β-HSD1 mRNA induced by TNFα or IL-1β [46 ± 10% ($P = 0.07$) and 41 ± 2% ($P < 0.01$), respectively]. This result indicates that induction of 11β-HSD1 by TNFα or IL-1β, at least in part, is attributable to the activation of SMase. Such an effect was not observed when treated with fumonisin B1 or myriocin (data not shown). These results raise a possibility that ceramide-mediated signaling pathway is involved in the regulation of 11β-HSD1 in preadipocytes.

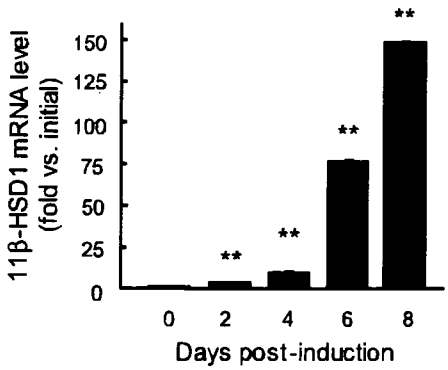

FIG. 1. Expression profile of 11β-HSD1 mRNA during the course of differentiation in 3T3-L1 cells. Postconfluent 3T3-L1 preadipocytes were induced to differentiate as described in *Materials and Methods*. mRNA level of 11β-HSD1 was determined. Results are means ± SEM from three experiments. **, $P < 0.01$ compared with 2 d postconfluent preadipocytes (initial).

Effect of ceramide on the expression of 11β-HSD1 in 3T3-L1 differentiated adipocytes

Induction of 11β-HSD1 mRNA by C_2 ceramide (10–100 μM) was not observed in 3T3-L1 differentiated adipocytes during 24-h incubation periods (Fig. 3A). Similarly, SMase (25–200 mU/ml) and S1P (1.0–10 μM) did not induce the expression of 11β-HSD1 (Fig. 3, B and C). These results are in agreement with our data that a robust induction of 11β-HSD1 expression by TNFα and IL-1β was observed only in 3T3-L1 preadipocytes but not in differentiated adipocytes (data not shown). Altogether, our data suggest that the effect of C_2 ceramide, SMase, and S1P on 11β-HSD1 expression is restricted in preadipocytes.

Effect of AICAR on the expression of 11β-HSD1 in 3T3-L1 preadipocytes

AMPK is activated by cellular stresses that interfere with ATP production (20–22). In contrast, 11β-HSD1 is a NADPH-dependent enzyme and its oxo-reductase activity requires NADPH supply from a glucose metabolizing pathway (36). This scheme tempted us to speculate that 11β-HSD1 would be involved in an AMPK-mediated fuel sensing mechanism. To test this hypothesis, we examined the effect of AMPK on the expression of 11β-HSD1 using a cell permeable AMP analog, AICAR (37).

When 3T3-L1 preadipocytes were treated with AICAR (0.1–0.5 mM) for 24 h, AMPK phosphorylation was increased pronouncedly (Fig. 4A). MCP-1 mRNA level was not altered even after the treatment with AICAR (Fig. 4B). In contrast, 11β-HSD1 mRNA level was increased in a dose-dependent manner, reaching to 8.7 ± 0.8-fold ($P < 0.05$) (Fig. 4C). Oxo-reductase activity of 11β-HSD1 was concomitantly increased by 3.0 ± 0.2-fold ($P < 0.01$) after the treatment with 0.5 mM AICAR (Fig. 4D).

To further evaluate the involvement of AMPK in the regulation of 11β-HSD1, cells were cotreated with AICAR and a selective AMPK inhibitor, compound C (38). Western blot analyses showed that augmented phosphorylation of AMPK and ACC by the treatment with 0.5 mM AICAR were attenuated when cells were cotreated with 10 μM compound C (Fig. 5A). Compound C completely blocked the effect of 0.5 mM AICAR on its augmentation of 11β-HSD1 (80 ± 2.4% decrease compared with AICAR-treated group, $P < 0.01$) (Fig. 5B). These results indicate that augmented expression of 11β-HSD1 by AICAR largely is attributable to the activation of AMPK. In contrast, mRNA of glucocorticoid receptor, which is known to express considerably in preadipocytes (39), was not affected by AICAR or compound C (data not shown).

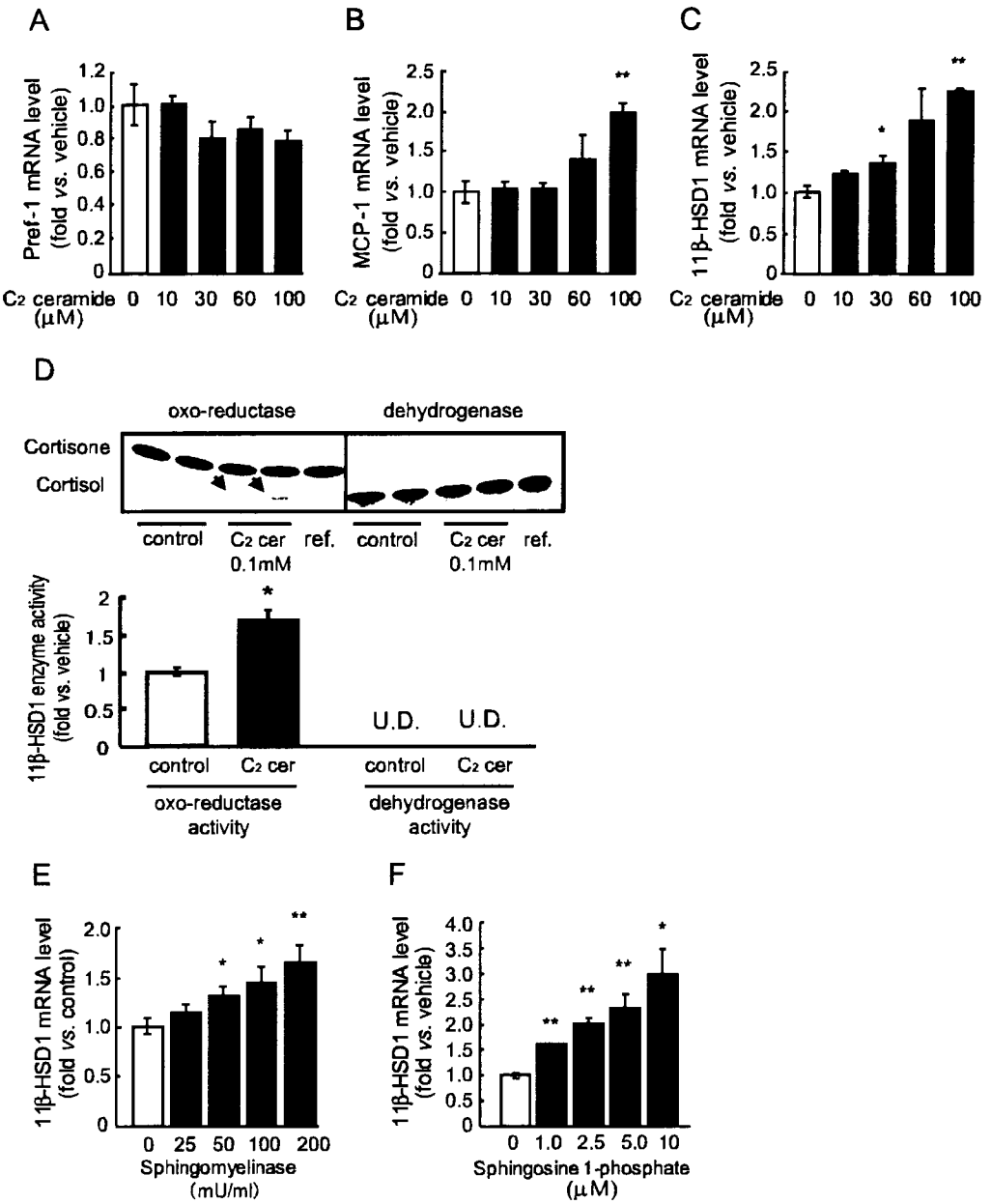

FIG. 2. Ceramide induces the expression of 11β-HSD1 in 3T3-L1 preadipocytes. A–D, Cells were treated with C_2 ceramide (10–100 μM) for 24 h. mRNA level of Pref-1 (A), MCP-1 (B), and 11β-HSD1 (C). D, Assay for 11β-HSD1 enzyme activity. Cells treated with C_2 ceramide (100 μM) for 24 h were subsequently incubated in serum-free media containing 250 nM of cortisone or cortisol with tritium-labeled tracer (6.4 μCi/ml of [1,2-^{3}H]$_2$ cortisone or [1,2,6,7-^{3}H]$_4$ cortisol) for 12 h. Emerged spots of cortisol are indicated by *arrows*. E and F, mRNA level of 11β-HSD1 after treatment with bacterial SMase (25–200 mU/ml) (E) and S1P (1.0–10 μM) (F) for 24 h. Results are means ± SEM from three experiments. *, $P < 0.05$, **, $P < 0.01$ compared with vehicle-treated group. U.D., Under detectable.

Effects of ceramide and AMPK signaling on the expression of 11β-HSD1 in human preadipocytes

To explore whether potent effects of ceramide and AMPK on 11β-HSD1 expression are reproduced in human preadipocytes (25, 26), impact of C_2 ceramide, S1P, and AICAR on 11β-HSD1 expression and enzyme activity were similarly analyzed. When cells were treated with C_2 ceramide (25–100 μM) for 24 h, 11β-HSD1 mRNA level was increased dose dependently, reaching to 5.3 ± 0.3-fold ($P < 0.01$) (Fig. 6A). In contrast, the effect of S1P (2.5–10 μM) was marginal (Fig. 6A). AICAR (0.3–1.0 mM) induced the phosphorylation of AMPK (Fig. 6B) and augmented 11β-HSD1 mRNA level by 2.8 ± 0.1-fold ($P < 0.01$) (Fig. 6A). C_2 ceramide (50 μM) and AICAR (1.0 mM) significantly increased the oxo-reductase activity of 11β-HSD1 by 2.9 ± 0.3-fold ($P < 0.01$) and 2.1 ± 0.04-fold ($P < 0.05$) (Fig. 6C).

Induction of C/EBPβ by ceramide and AMPK signaling in 3T3-L1 preadipocytes

11β-HSD1 promoter contains a couple of C/EBP binding sites, and C/EBP mediated regulation of 11β-HSD1 has long

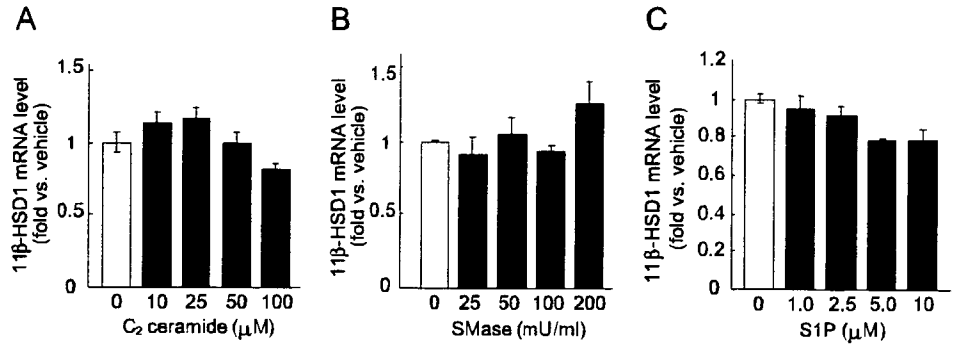

FIG. 3. Ceramide does not influence the expression of 11β-HSD1 in differentiated 3T3-L1 adipocytes. mRNA level of 11β-HSD1 after treatment with C_2 ceramide (10–100 μM) (A), SMase (25–200 mU/ml) (B), and S1P (1.0–10 μM) (C) for 24 h. Results are means ± SEM from three independent experiments.

been investigated exclusively in hepatocytes (40). Because C/EBPα is not expressed in preadipocytes (41), we tested a possibility that C/EBPβ would be involved in the regulation of 11β-HSD1 by ceramide or AICAR. Western blot analysis showed that C/EBPβ expression was substantially increased after the treatment with C_2 ceramide (0.1 mM) or AICAR (0.5 mM), culminating in 1.8- and 6.5-fold increase within 3 h, respectively (Fig. 7, A and B). Expression of C/EBPβ by C_2 ceramide or AICAR was increased in a dose-dependent manner (data not shown). In contrast, 11β-HSD1 expression was induced 12 h after the treatment with C_2 ceramide or AICAR (data not shown).

To explore a possible involvement of C/EBPβ in 11β-HSD1 regulation, ChIP analysis was performed with primers spanning putative C/EBP binding sites in mouse 11β-HSD1 promoter (30). No amplified band was observed in samples processed without antibody (No antibody control), excluding a possibility of nonspecific binding between DNA fragments and protein A-agarose (Fig. 7C). When treated with C_2 ceramide or AICAR for 6 h, association of C/EBPβ with the promoter of 11β-HSD1 gene was substantially induced (Fig. 7C). Our data demonstrated that the activation of ceramide or AMPK pathways induced the expression of C/EBPβ and its binding to the 11β-HSD1 promoter.

Effect of C/EBPβ knockdown on the expression of 11β-HSD1 induced by ceramide or AMPK signaling in 3T3-L1 preadipocytes

To further validate a role of C/EBPβ in the control of 11β-HSD1 by ceramide or AICAR, C/EBPβ protein was transiently knocked down by siRNA. When 3T3-L1 preadipocytes were transfected with siRNA, C/EBPβ protein expression induced by C_2 ceramide or AICAR was markedly attenuated, demonstrating effective silencing of C/EBPβ (Fig. 8, A and B). Notably, augmented expression of 11β-HSD1 induced by C_2 ceramide or AICAR was significantly attenuated in cells transfected with C/EBPβ siRNA (Fig. 8,

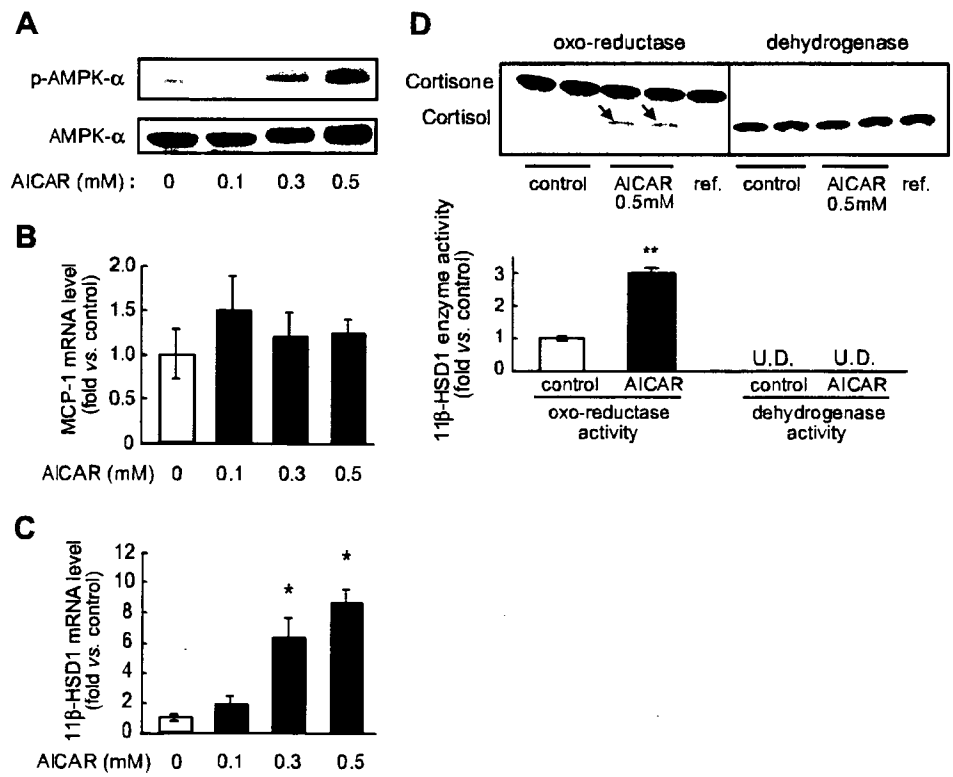

FIG. 4. AMPK activation enhances the expression of 11β-HSD1 in 3T3-L1 preadipocytes. Cells were treated with AICAR (0.1–0.5 mM) for 24 h. A, Western blot of AMPK protein and phosphorylated AMPK (p-AMPK). mRNA levels of MCP-1 (B) and 11β-HSD1 (C). D, Assay for 11β-HSD1 activity. Cells treated with AICAR (0.5 mM) for 24 h were incubated in serum-free media containing 250 nM of cortisone or cortisol with tritium-labeled tracer (6.4 μCi/ml of [1,2-^{3}H]$_2$ cortisone or [1,2,6,7-^{3}H]$_4$ cortisol) for 12 h. Emerged spots of cortisol were indicated by *arrows*. Results are means ± SEM from three or four experiments. *, $P < 0.05$, **, $P < 0.01$ compared with control (cells without AICAR treatment) group. U.D., Under detectable.

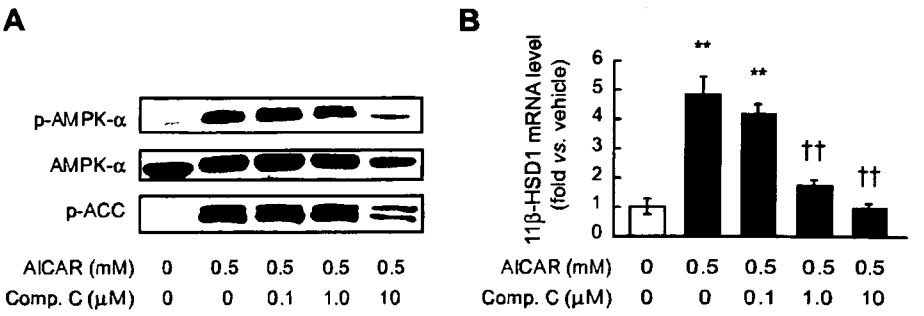

FIG. 5. AICAR-induced expression of 11β-HSD1 is attenuated by an AMPK inhibitor. 3T3-L1 preadipocytes were cotreated with AICAR (0.5 mM) and indicated concentrations of compound C (Comp. C) for 24 h. A, Western blot of total AMPK protein, phosphorylated AMPK (p-AMPK) and phosphorylated ACC (p-ACC). B, mRNA level of 11β-HSD1. Results are means ± SEM from three experiments. **, $P < 0.01$ compared with vehicle-treated group. ††, $P < 0.01$ compared with AICAR-treated group.

C and D). In contrast, negative control Stealth RNAi treatment had no impact on the expression of C/EBPβ or 11β-HSD1. These results suggest that C/EBPβ is involved critically in the induction of 11β-HSD1 by ceramide- or AMPK-mediated signaling pathways.

Discussion

The major finding of the present study is that ceramide- and AMPK-mediated signaling pathways augment the expression and enzyme activity of 11β-HSD1 in both murine and human preadipocytes. We provide novel evidence that activation of ceramide and AMPK pathways induce the expression of C/EBPβ. ChIP analyses demonstrate the DNA binding of C/EBPβ to 11β-HSD1 promoter, and transient knockdown of C/EBPβ protein by siRNA further support the notion that C/EBPβ is critically involved in the expression of 11β-HSD1 induced by C_2 ceramide or AICAR. Taken together, the present study highlights a novel mechanism that metabolic stress-related signaling pathways mediated by ceramide and AMPK regulate the expression of 11β-HSD1 in preadipocytes.

Ceramide acts as a lipid mediator of metabolic stress response (18, 42). Fatty acids, proinflammatory cytokines, glucocorticoids, and serum deprivation in cultured cells are known to induce intracellular accumulation of ceramide (43, 44). Importantly, aberrant accumulation of ceramide in insulin target tissues appreciably contributes to local insulin resistance and underlies, at least partly, the molecular mechanism of lipotoxicity (43, 44). A recent study demonstrated that mRNA level of enzymes involved in sphingolipid metabolism in adipose tissue as well as plasma level of SMase, ceramide, sphingosine, and S1P were increased in *ob/ob* mice (45). Thus we tested a possibility whether 11β-HSD1 would be induced by ceramide signals in preadipocytes. In this context, the present study is the first to demonstrate that the expression of 11β-HSD1 was induced by C_2 ceramide, bacterial SMase and S1P in preadipocytes (Fig. 2). In contrast, induction of 11β-HSD1 expression by C_2 ceramide, SMase, and S1P was not observed in differentiated adipocytes (Fig. 3), suggesting that such effects are restricted in preadipocytes.

SMase catalyzes the hydrolysis of sphingomyelin in outer side of the plasma membrane, leading to the production of ceramide (19). Ceramide is subsequently metabolized to S1P, which functions through S1P receptors (19). In the present study, we found that inhibition of SMase by desipramine attenuated the TNFα- or IL-1β-induced expression of 11β-HSD1. This observation is in agreement with previous reports that TNFα and IL-1β promptly induced the hydrolysis of sphingomyelin to generate ceramide (46). Assays in the present study are validated by the finding that expression of MCP-1 was induced by C_2 ceramide (Fig. 2), consistent with the notion that NFκB and MAPK signaling pathways are involved in the regulation of MCP-1 (47) and that ceramide and S1P potently mediate NFκB and MAPK pathways (18, 48).

In the present study, C_2 ceramide induced the expression of 11β-HSD1 at 50–100 μM (Fig. 2). It has been reported that the physiological concentration of ceramide within cells are approximately 1–5 μM (49). Accordingly, C_2 ceramide does induce biological effects including differentiation and growth inhibition at 1–5 μM in serum-free media. However, higher concentration (50–100 μM) of C_2 ceramide are required to induce equipotent effects in serum-containing medium, because serum proteins bind C_2 ceramide and reduce its potency (50), and for this, 50–100 μM C_2 ceramide has been commonly used in many previous studies (51, 52). It should also be noted that, because ceramide resides in "lipid rafts" in the membrane (53), local concentration of ceramide within cells must be much higher than 5 μM. In this context, the concentration of C_2 ceramide used in the present study is appropriate for analyzing the responsiveness of ceramide in adipocytes.

AMPK, activated by the increase in intracellular AMP level, plays a crucial role in mediating cellular stress such as hypoxia, glucose deprivation, and ischemia (20–22). Recent studies highlighted a potential role of AMPK in regulating energy balance and mass of adipose tissue (23, 24). ATP level of adipose tissue is decreased in obese rodent models (54), supporting the notion that local hypoxia and inflammation is associated with defective energy metabolism in obese adipose tissue (14, 54). In this context, the present study demonstrates for the first time that AICAR markedly augmented the expression of 11β-HSD1 in preadipocytes (Fig. 4). Furthermore, a potent AMPK inhibitor compound C completely suppressed the induction of 11β-HSD1 (Fig. 5), verifying that AMPK signaling pathway is involved in the regulation of 11β-HSD1. Based on the present study in 3T3-L1 preadipocytes (Figs. 2, 4, and 5), a potential interaction between ceramide and AMPK in terms of the effect on 11β-HSD1 expression would be of considerable interest. In 3T3-L1 preadipocytes, AMPK was not activated when treated with C_2 ceramide (data not shown). Although further studies are required, these results suggest that ceramide signal is not directly involved in AMPK-mediated induction of 11β-HSD1.

The present study is the first to demonstrate that C_2 cer-

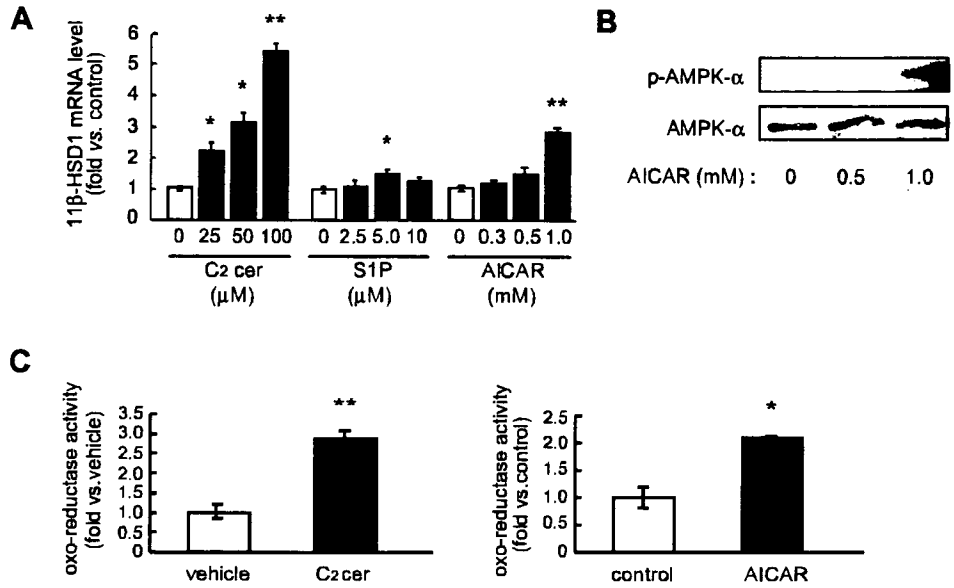

FIG. 6. Ceramide and AMPK signaling induces the expression of 11β-HSD1 in human preadipocytes. Human preadipocytes were treated with C_2 ceramide (C_2cer, 25–100 μM), S1P (2.5–10 μM) and AICAR (0.3–1.0 mM) for 24 h. A, mRNA levels of 11β-HSD1 were determined. B, Western blot of AMPK protein and phosphorylated AMPK (p-AMPK) after treatment with AICAR for 3 h. C, Assay for 11β-HSD1 oxo-reductase activity. Cells were treated with C_2 ceramide (50 μM, *left*) or AICAR (1.0 mM, *right*) for 24 h, and subsequently incubated with tritium-labeled cortisone for 12 h. Results are means ± SEM from three experiments. *, $P < 0.05$, **, $P < 0.01$ compared with control or vehicle-treated group.

amide and AICAR augmented the expression of C/EBPβ in 3T3-L1 preadipocytes (Fig. 7). This result is consistent with a line of previous reports showing that S1P induced phosphorylation of cAMP-responsive-element-binding protein (CREB) (48), and CREB potentially controls the expression of C/EBPβ in adipocytes (55). Furthermore, the present study is the first demonstration that the activation of AMPK induced the expression of C/EBPβ in any kinds of cells. It is well-characterized that transient expression of C/EBPβ is essential for the induction of PPARγ and C/EBPα in the early phase of adipogenesis (41). A recent report raised a possibility that AICAR inhibited adipogenesis by interfering induction of PPARγ and C/EBPα (56). Therefore, it is tempting to speculate that AMPK-induced augmentation and sustainment of C/EBPβ and resultant suppression of adipogenesis may be a facet of adaptation to nutritional threat.

Compared with murine adipocytes, the mechanism responsible for adipogenesis and adipokine secretion is poorly understood in humans (57). For example, human preadipocytes do not require the process of clonal expansion in the course of adipogenesis (57). Therefore, we examined the effect of ceramide and AMPK signaling on the expression of 11β-HSD1 using human preadipocytes. The present study demonstrates that sphingolipids (C_2 ceramide and S1P) and AICAR induced the expression of 11β-HSD1 also in human preadipocytes (Fig. 6). The effect of C_2 ceramide was exaggerated in human preadipocytes compared with 3T3-L1 preadipocytes, whereas the effect of S1P was mild in human preadipocytes. Treatment of C_2 ceramide did not affect MCP-1 mRNA level, but AICAR substantially reduced the expression in a dose-dependent manner (data not shown), representing a contrast to the data in 3T3-L1 preadipocytes (Figs. 2 and 4). Even considering differences in cell types or species (58), our data provide novel evidence that ceramide and AMPK signals induce the expression of 11β-HSD1 in both rodent and human cultured preadipocytes. Recent

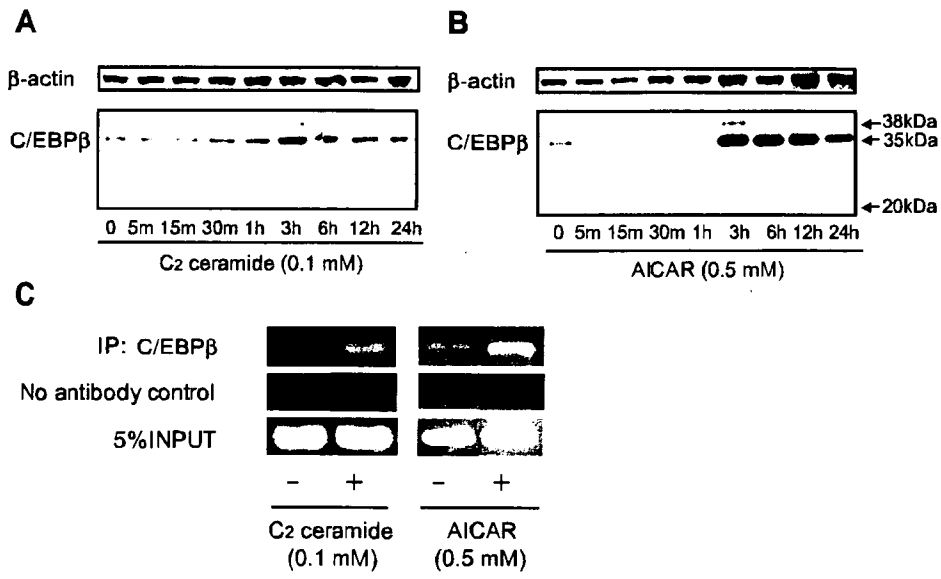

FIG. 7. Ceramide and AICAR induce the expression of C/EBPβ in 3T3-L1 preadipocytes. Western blot of C/EBPβ after the treatment with 0.1 mM C_2 ceramide (A) or 0.5 mM AICAR (B). β-Actin was used as a loading control. ChIP analysis after the treatment with 0.1 mM C_2 ceramide or 0.5 mM AICAR for 6 h (C). Chromatin-associated DNA was immunoprecipitated with an antibody against C/EBPβ. The immunoprecipitated DNA, samples processed without antibody (indicated as No antibody control), and 5% amount of sonicated DNA (indicated as 5% INPUT) were subjected to PCR using specific primers for 11β-HSD1 promoter region. Amplified DNA indicates the binding of C/EBPβ to the 11β-HSD1 promoter.

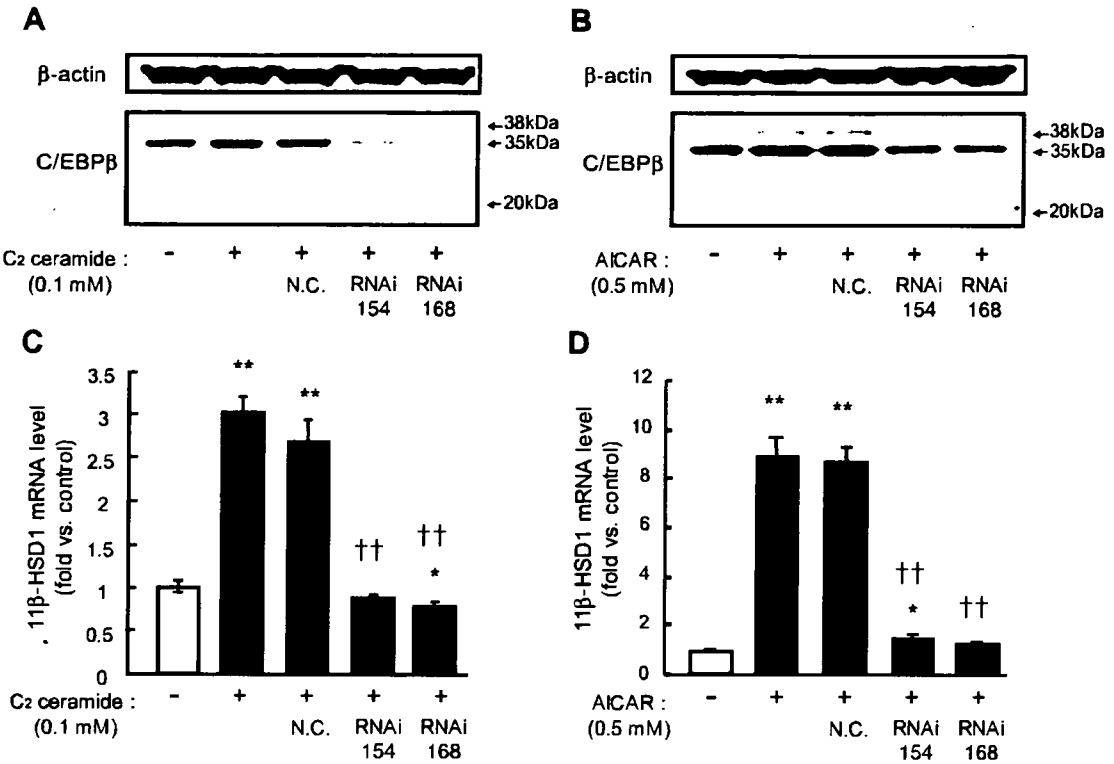

FIG. 8. Effect of C/EBPβ knockdown on C_2 ceramide- or AICAR-induced expression of 11β-HSD1 in 3T3-L1 preadipocytes. Cells were transfected with either Stealth RNAi negative control (N.C.) or C/EBPβ Stealth RNAi (RNAi154, RNAi168). After 12 h of incubation, cells were treated with C_2 ceramide or AICAR. Western blot of C/EBPβ after the treatment with 0.1 mM C_2 ceramide (A) or 0.5 mM AICAR (B) for 3 h. β-Actin was used as a loading control. mRNA level of 11β-HSD1 after the treatment with 0.1 mM C_2 ceramide (C) or 0.5 mM AICAR (D) for 24 h. Results are means ± SEM from four experiments. *, $P < 0.05$, **, $P < 0.01$ compared with control group. ††, $P < 0.01$ compared with C_2 ceramide or AICAR-treated group.

works demonstrated that human adipose tissue contained a considerable amount of preadipocytes (59, 60), which may be involved in some aspects of adipose tissue function (15, 60). In this context, further *in vivo* studies are warranted to validate the possible involvement of ceramide and AMPK signals in 11β-HSD1 regulation in human preadipocytes.

C/EBP family of transcription factors (C/EBPs) in adipocytes serve as master regulators of a variety of cellular response (61), and expression of C/EBPs is regulated by a variety of hormones, cytokines, and nutrients (61, 62). 11β-HSD1 promoter contains a couple of C/EBP binding sites, and previous studies demonstrated that the expression of 11β-HSD1 was controlled by C/EBPs (40, 63). In this context, the present study demonstrates, for the first time, that induction of C/EBPβ in preadipocytes was observed around 3 h after the treatment with C_2 ceramide or AICAR (Fig. 7), which preceded the robust induction of 11β-HSD1. Our data of ChIP analyses and C/EBPβ knockdown experiments further reinforced the notion that C/EBPβ is involved in ceramide- and AMPK-mediated augmentation of 11β-HSD1 in preadipocytes (Figs. 7 and 8).

It should be noted that glucocorticoid is known to increase the expression and activity of SMase, resulting in intracellular ceramide accumulation and local insulin resistance (43). This notion prompts us to speculate a vicious cycle within cells where ceramide and 11β-HSD1-derived active glucocorticoid reciprocally aggravate preadipocyte dysfunction. Unexpected regulation of 11β-HSD1 by AMPK pathway may also provide a novel clue to better understand molecular pathophysiology of adipose dysfunction. Collectively, the present study is the first demonstration that ceramide and AMPK signaling pathways augment the expression and enzyme activity of 11β-HSD1 in human and rodent preadipocytes, thereby highlighting a metabolic stress-related regulation of 11β-HSD1 in a cell-specific manner.

Acknowledgments

We thank Ms. S. Maki, K. Koyama, and M. Nagamoto for experimental assistance. We are grateful to Dr. S. Yokota and Mr. Y. Tominaga (Kaneka Corporation) for technical advice.

Received March 14, 2007. Accepted August 8, 2007.

Address all correspondence and requests for reprints to: Hiroaki Masuzaki, M.D., Ph.D., Division of Endocrinology and Metabolism, Department of Medicine and Clinical Science, Kyoto University Graduate School of Medicine, 54, Shogoin Kawahara-cho, Sakyo-ku, Kyoto 606-8507, Japan. E-mail: hiroaki@kuhp.kyoto-u.ac.jp.

This work was supported by Grant-in-Aid for Scientific Research (B2) (16390267); Grant-in-Aid for Scientific Research (S2) (16109007); Grant-in-Aid for Scientific Research on Priority Areas (Adipomics, 15081101); Grant-in-Aid for Research on Measures for Intractable Diseases (Health and Labor Science Research Grant); The Ministry of Education, Culture, Sports, Science and Technology of Japan; Research Grant from Special Coordination Funds for Promoting Science and Technology (Japan Science and Technology Agency); AstraZeneca International Research Grant; Takeda Medical Research Foundation; Smoking Research Foundation; Setsuro Fujii Memorial Osaka Foundation for Promotion of Fun-

damental Medical Research; Research Grant for Cardiovascular Diseases (National Cardiovascular Center); Mitsubishi Pharma Research Foundation; and Sankyo Research Foundation for Medical Research.

Disclosure Statement: The authors of this manuscript have nothing to disclose.

References

1. **Grundy SM, Brewer Jr HB, Cleeman JI, Smith Jr SC, Lenfant C** 2004 Definition of metabolic syndrome: report of the National Heart, Lung, and Blood Institute/American Heart Association conference on scientific issues related to definition. Circulation 109:433–438
2. **Matsuzawa Y** 2006 Therapy insight: adipocytokines in metabolic syndrome and related cardiovascular disease. Nat Clin Pract Cardiovasc Med 3:35–42
3. **Masuzaki H, Paterson J, Shinyama H, Morton NM, Mullins JJ, Seckl JR, Flier JS** 2001 A transgenic model of visceral obesity and the metabolic syndrome. Science 294:2166–2170
4. **Masuzaki H, Yamamoto H, Kenyon CJ, Elmquist JK, Morton NM, Paterson JM, Shinyama H, Sharp MG, Fleming S, Mullins JJ, Seckl JR, Flier JS** 2003 Transgenic amplification of glucocorticoid action in adipose tissue causes high blood pressure in mice. J Clin Invest 112:83–90
5. **Kotelevtsev Y, Holmes MC, Burchell A, Houston PM, Schmoll D, Jamieson P, Best R, Brown R, Edwards CR, Seckl JR, Mullins JJ** 1997 11β-Hydroxysteroid dehydrogenase type 1 knockout mice show attenuated glucocorticoid inducible responses and resist hyperglycemia on obesity or stress. Proc Natl Acad Sci USA 94:14924–14929
6. **Morton NM, Holmes MC, Fievet C, Staels B, Tailleux A, Mullins JJ, Seckl JR** 2001 Improved lipid and lipoprotein profile, hepatic insulin sensitivity, and glucose tolerance in 11β-hydroxysteroid dehydrogenase type 1 null mice. J Biol Chem 276:41293–41300
7. **Morton NM, Paterson JM, Masuzaki H, Holmes MC, Staels B, Fievet C, Walker BR, Flier JS, Mullins JJ, Seckl JR** 2004 Novel adipose tissue-mediated resistance to diet-induced visceral obesity in 11 β-hydroxysteroid dehydrogenase type 1 deficient mice. Diabetes 53:931–938
8. **Seckl JR, Walker BR** 2001 Minireview: 11β hydroxysteroid dehydrogenase type 1—a tissue-specific amplifier of glucocorticoid action. Endocrinology 142:1371–1376
9. **Bujalska IJ, Kumar S, Stewart PM** 1997 Does central obesity reflect "Cushing's disease of the omentum"? Lancet 349:1210–1213
10. **Wake DJ, Rask E, Livingstone DE, Soderberg S, Olsson T, Walker BR** 2003 Local and systemic impact of transcriptional up-regulation of 11β-hydroxysteroid dehydrogenase type 1 in adipose tissue in human obesity. J Clin Endocrinol Metab 88:3983–3988
11. **Alberts P, Nilsson C, Selen G, Engblom LO, Edling NH, Norling S, Klingstrom G, Larsson C, Forsgren M, Ashkzari M, Nilsson CE, Fiedler M, Bergqvist E, Ohman B, Bjorkstrand E, Abrahmsen LB** 2003 Selective inhibition of 11 β-hydroxysteroid dehydrogenase type 1 improves hepatic insulin sensitivity in hyperglycemic mice strains. Endocrinology 144:4755–4762
12. **Hermanowski-Vosatka A, Balkovec JM, Cheng K, Chen HY, Hernandez M, Koo GC, Le Grand CB, Li Z, Metzger JM, Mundt SS, Noonan H, Nunes CN, Olson SH, Pikounis B, Ren N, Robertson N, Schaeffer JM, Shah K, Springer MS, Strack AM, Strowski M, Wu K, Wu T, Xiao J, Zhang BB, Wright SD, Thieringer R** 2005 11β-HSD1 inhibition ameliorates metabolic syndrome and prevents progression of atherosclerosis in mice. J Exp Med 202:517–527
13. **Cinti S, Mitchell G, Barbatelli G, Murano I, Ceresi E, Faloia E, Wang S, Fortier M, Greenberg AS, Obin MS** 2005 Adipocyte death defines macrophage localization and function in adipose tissue of obese mice and humans. J Lipid Res 46:2347–2355
14. **Neels JG, Olefsky JM** 2006 Inflamed fat: what starts the fire? J Clin Invest 116:33–35
15. **Tchkonia T, Giorgadze N, Pirtskhalava T, Thomou T, DePonte M, Koo A, Forse RA, Chinnappan D, Martin-Ruiz C, von Zglinicki T, Kirkland JL** 2006 Fat depot specific characteristics are retained in strains derived from single human preadipocytes. Diabetes 55:2571–2578
16. **Schaffler A, Scholmerich J, Buchler C** 2005 Mechanisms of disease: adipocytokines and visceral adipose tissue—emerging role in intestinal and mesenteric diseases. Nat Clin Pract Gastroenterol Hepatol 2:103–111
17. **Paulmyer-Lacroix O, Boullu S, Oliver C, Alessi MC, Grino M** 2002 Expression of the mRNA coding for 11β hydroxysteroid dehydrogenase type 1 in adipose tissue from obese patients: an in situ hybridization study. J Clin Endocrinol Metab 87:2701–2705
18. **Mathias S, Pena LA, Kolesnick RN** 1998 Signal transduction of stress via ceramide. Biochem J 335(Pt 3):465–480
19. **Tani M, Ito M, Igarashi Y** 2006 Ceramide/sphingosine/sphingosine 1-phosphate metabolism on the cell surface and in the extracellular space. Cell Signal 19:229–237
20. **Minokoshi Y, Kim YB, Peroni OD, Fryer LG, Muller C, Carling D, Kahn BB** 2002 Leptin stimulates fatty-acid oxidation by activating AMP-activated protein kinase. Nature 415:339–343
21. **Hardie DG** 2003 Minireview: the AMP-activated protein kinase cascade: the key sensor of cellular energy status. Endocrinology 144:5179–5183
22. **Tanaka T, Hidaka S, Masuzaki H, Yasue S, Minokoshi Y, Ebihara K, Chusho H, Ogawa Y, Toyoda T, Sato K, Miyanaga F, Fujimoto M, Tomita T, Kusakabe T, Kobayashi N, Tanioka H, Hayashi T, Hosoda K, Yoshimatsu H, Sakata T, Nakao K** 2005 Skeletal muscle AMP activated protein kinase phosphorylation parallels metabolic phenotype in leptin transgenic mice under dietary modification. Diabetes 54:2363–2374
23. **Dagon Y, Avraham Y, Berry EM** 2006 AMPK activation regulates apoptosis, adipogenesis, and lipolysis by eIF2α in adipocytes. Biochem Biophys Res Commun 340:43–47
24. **Gaidhu MP, Fediuc S, Ceddia RB** 2006 5-Aminoimidazole-4-carboxamide 1-β-D-ribofuranoside induced AMP activated protein kinase phosphorylation inhibits basal and insulin stimulated glucose uptake, lipid synthesis, and fatty acid oxidation in isolated rat adipocytes. J Biol Chem 281:25956–25964
25. **Wang M, Crisostomo PR, Herring C, Meldrum KK, Meldrum DR** 2006 Human progenitor cells from bone marrow or adipose tissue produce VEGF, HGF, and IGF I in response to TNF by a p38 MAPK dependent mechanism. Am J Physiol Regul Integr Comp Physiol 291:R880–R884
26. **Benson SC, Pershadsingh HA, Ho CI, Chittiboyina A, Desai P, Pravenec M, Qi N, Wang J, Avery MA, Kurtz TW** 2004 Identification of telmisartan as a unique angiotensin II receptor antagonist with selective PPARγ-modulating activity. Hypertension 43:993–1002
27. **Fujimoto M, Masuzaki H, Tanaka T, Yasue S, Tomita T, Okazawa K, Fujikura J, Chusho H, Ebihara K, Hayashi T, Hosoda K, Nakao K** 2004 An angiotensin II AT1 receptor antagonist, telmisartan augments glucose uptake and GLUT4 protein expression in 3T3-L1 adipocytes. FEBS Lett 576:492–497
28. **Li J, Coven DL, Miller EJ, Hu X, Young ME, Carling D, Sinusas AJ, Young LH** 2006 Activation of AMPK α- and γ-isoform complexes in the intact ischemic rat heart. Am J Physiol Heart Circ Physiol 291:H1927–H1934
29. **Salt IP, Connell JM, Gould GW** 2000 5-Aminoimidazole-4-carboxamide ribonucleoside (AICAR) inhibits insulin-stimulated glucose transport in 3T3-L1 adipocytes. Diabetes 49:1649–1656
30. **Voice MW, Seckl JR, Chapman KE** 1999 The sequence of 5′ flanking DNA from the mouse 11β-hydroxysteroid dehydrogenase type 1 gene and analysis of putative transcription factor binding sites. Gene 181:233–235
31. **Smas CM, Sul HS** 1993 Pref-1, a protein containing EGF-like repeats, inhibits adipocyte differentiation. Cell 73:725–734
32. **Boney CM, Fiedorek Jr FT, Paul SR, Gruppuso PA** 1996 Regulation of preadipocyte factor-1 gene expression during 3T3-L1 cell differentiation. Endocrinology 137:2923–2928
33. **Wang E, Norred WP, Bacon CW, Riley RT, Merrill Jr AH** 1991 Inhibition of sphingolipid biosynthesis by fumonisins. Implications for diseases associated with Fusarium moniliforme. J Biol Chem 266:14486–14490
34. **Miyake Y, Kozutsumi Y, Nakamura S, Fujita T, Kawasaki T** 1995 Serine palmitoyltransferase is the primary target of a sphingosine-like immunosuppressant, ISP-1/myriocin. Biochem Biophys Res Commun 211:396–403
35. **Albouz S, Hauw JJ, Berwald-Netter Y, Boutry JM, Bourdon R, Baumann N** 1981 Tricyclic antidepressants induce sphingomyelinase deficiency in fibroblast and neuroblastoma cell cultures. Biomedicine 35:218–220
36. **McCormick KL, Wang X, Mick GJ** 2006 Evidence that the 11 β-hydroxysteroid dehydrogenase (11 β-HSD1) is regulated by pentose pathway flux. Studies in rat adipocytes and microsomes. J Biol Chem 281:341–347
37. **Corton JM, Gillespie JG, Hawley SA, Hardie DG** 1995 5-Aminoimidazole-4-carboxamide ribonucleoside. A specific method for activating AMP-activated protein kinase in intact cells? Eur J Biochem 229:558–565
38. **Zhou G, Myers R, Li Y, Chen Y, Shen X, Fenyk-Melody J, Wu M, Ventre J, Doebber T, Fujii N, Musi N, Hirshman MF, Goodyear LJ, Moller DE** 2001 Role of AMP-activated protein kinase in mechanism of metformin action. J Clin Invest 108:1167–1174
39. **Floyd ZE, Stephens JM** 2003 STAT5A promotes adipogenesis in nonprecursor cells and associates with the glucocorticoid receptor during adipocyte differentiation. Diabetes 52:308–314
40. **Williams LJ, Lyons V, MacLeod I, Rajan V, Darlington GJ, Poli V, Seckl JR, Chapman KE** 2000 C/EBP regulates hepatic transcription of 11β hydroxysteroid dehydrogenase type 1. A novel mechanism for cross talk between the C/EBP and glucocorticoid signaling pathways. J Biol Chem 275:30232–30239
41. **Tang QQ, Zhang JW, Lane DM** 2004 Sequential gene promoter interactions of C/EBPβ, C/EBPα, and PPARγ during adipogenesis. Biochem Biophys Res Commun 319:235–239
42. **Sawai H, Okazaki T, Yamamoto H, Okano H, Takeda Y, Tashima M, Sawada H, Okuma M, Ishikura H, Umehara H, Domae N** 1995 Requirement of AP-1 for ceramide induced apoptosis in human leukemia HL-60 cells. J Biol Chem 270:27326–27331
43. **Summers SA, Nelson DH** 2005 A role for sphingolipids in producing the common features of type 2 diabetes, metabolic syndrome X, and Cushing's syndrome. Diabetes 54:591–602
44. **Chavez JA, Holland WL, Bar J, Sandhoff K, Summers SA** 2005 Acid ceramidase overexpression prevents the inhibitory effects of saturated fatty acids on insulin signaling. J Biol Chem 280:20148–20153
45. **Samad F, Hester KD, Yang G, Hannun YA, Bielawski J** 2006 Altered adipose and plasma sphingolipid metabolism in obesity: a potential mechanism for cardiovascular and metabolic risk. Diabetes 55:2579–2587
46. **Andrieu N, Salvayre R, Jaffrezou JP, Levade T** 1995 Low temperatures and